Reviewer 1

This study investigates the impact of aerosols on ice crystal effective radius (Rei) by using satellite data and parcel model. It reveals the different dependencies of Rei and aerosol optical depth (AOD) under high relative humidity (RH) regime and low RH regime. The mechanisms to cause the difference are discussed and approved by parcel model. The results would help better understand ice cloud microphysical process and better estimation of climate effect of aerosols. In general, the manuscript is well organized. Thus, I suggest a minor revision before publication.

Response: We thank the reviewer for the valuable comments. We have followed these comments in revising the manuscript. Point-to-point responses are given below.

The suggestions are list as following:

1. Rei from satellite data retrievals are based on the reflectance of two wavelength (Platnick et al., 2015). Satellite data retrievals need some assumptions and may have some uncertainties. For examples, the surface spectral albedo data is needed to get the retrievals results. This study focuses on East Asia and surrounding areas, for which most regions are land area. Land surface albedo data may have larger uncertainty, compared with ocean surface albedo. Moreover, a gamma particle size distribution consisting of severely-roughened aggregated column is used in satellite data retrievals (Platnick et al., 2015). Single scattering albedo (SSA) and asymmetric factor needed for retrievals are based on this assumption. Do you think how do these uncertainties affects the results in this study?

Response: Thank you for the comments. The MODIS team has performed a comprehensive assessment of the pixel-level uncertainty in R_{ei} retrievals, which has been incorporated in the Collection 6 Level 2 cloud product (MYD06). This uncertainty evaluation takes into account a variety of error sources, including 1) instrument calibration, 2) atmospheric corrections, 3) surface spectral reflectance, and 4) forward radiative transfer model, e.g., the size distribution assumption (Platnick et al., 2015). The pixel-level R_{ei} uncertainties for the samples used in this study are 6.41% ± 4.97% (standard deviation). We used mean R_{ei} within certain AOD bins and the uncertainties are smaller than those for individual pixels. Also, we focus on R_{ei} changes in response to aerosol loading instead of absolute R_{ei} values. For these reasons, the R_{ei} uncertainty ranges are much smaller than the magnitude of R_{ei} trends depicted in our study (Figs. 1 and 3). We note that the current uncertainty evaluation has not considered the assumptions of ice crystal habit, which will be discussed in the response to the reviewer's second comment.

Following the reviewer's comment, we have added the discussion on the uncertainties of satellite retrieval of R_{ei} in the revised manuscript. (Page 3, Line 25 to Page 4, Line 4)

2. The particle in ice cloud may have different types and morphologies. For example, in WRF-CHEM, cloud ice, snow, and grapple are used. Platnick et al. (2015) also mentions "solid bullet rosettes" and "solid aggregate plates". Optical properties of each types of particle are quite different. Rei is based on gamma distribution of aggregated column in satellite data retrievals. Thus, the shift of Rei may be caused both by shift of particle size distribution and change of particle type. The types of ice particle formed by homogeneous nucleation and heterogeneous nucleation might be different. Do you think the different type of particle would also be a possible reason, besides the shift of size distributions?

Response: We thank the reviewer for this valuable comment. Based on previous studies (Bailey and Hallett, 2009; Lawson et al., 2006; Lynch et al., 2002), the habit of ice crystals is dependent on a number of factors, among which the most important one is temperature, followed by ice supersaturation ratio. In this study we focus on R_{ei} changes with aerosol loading, for which temperature does not appear to have noticeable effect. For supersaturation ratio, the formation of ice crystals under moist conditions (high RH, high CAPE, or negative U200) is dominated by homogeneous nucleation, therefore the ice supersaturation ratio surrounding ice crystals is usually very low and the ice habit is not likely to change significantly with aerosol loading. Under drier conditions (low RH, low CAPE, or positive U200), however, heterogeneous nucleation gradually takes over homogeneous nucleation with aerosol loading increase. Subsequently, the supersaturation ratio surrounding ice crystals would become higher, possibly leading to changes in ice crystal habit. Considering that a single habit (i.e., aggregated column) is assumed in the satellite retrieval algorithm, ice habit changes could possibly induce changes in the satellite-retrieved R_{ei}. However, this retrieval bias should not change our major conclusion about the aerosol impact on ice crystal size, which has been supported by the cloud parcel modeling used in this study.

It should be noted that satellite remote sensing of ice clouds focuses on bulk (averaged) quantity and it is apparent that a single complex rough aggregate shape gives a more consistent retrieval from different MODIS bands and has been adopted for the objective of global ice cloud retrieval. We respectfully submit that at the present time space remote sensing does not have the capability to differentiate ice crystal shapes. The quantitative assessment of the impact of ice crystal habit on satellite retrievals of R_{ei} is a very complicated and difficult task that merits further in-depth study. We have added these discussions in the revised manuscript. (Page 17, Line 13-30)

3. There are many small figures in Figure 1, Figure 3, Figure 4 and Figure 5. Some of them are used to support similar conclusions. Maybe the author could consider placing some of them into supplemental information for better understanding of readers.

Response: Following the reviewer's comment, we have moved some panels of the original Figs. 3 and 4 to the Supplementary Information (Fig. S4 in the revised manuscript). The remaining panels of these two figures are combined into Fig. 3 in the revised manuscript. For the analysis of the impact of different meteorological parameters, we would prefer to keep the current layout after careful consideration for two reasons. First, the key conclusion of water vapor modulation needs to be supported by the analysis with respect to multiple meteorological parameters, including RH, CAPE, and U200, instead of a single parameter. Second, it may be more convenient to the readers to put these figures in the main text so that they do not need to frequently switch between the main text and Supplementary Information.

4. The criteria for low RH and high RH in Figure 1 and Figure 3 are 45% and 65%. But the criteria for Figure 4 is 43% and 58%. Is there any reason for the differences? Will the criteria affect the statistic results?

Response: The probability distributions of RH (as well as other meteorological parameters) are different for convection-generated and in-situ ice clouds. We used different thresholds so that there are approximately the same samples in each meteorological range. We have also tried to apply the same breaking points for both ice cloud types, and found that the R_{ei}-aerosol relation patterns are retained, but the error bars are larger for some meteorological ranges containing fewer samples.

5. In parcel model results part, water vapor mass mixing ratios and aerosol number concentration are used, which are different from satellite data part, i.e., AOD and RH. Is it possible to use same variables for better comparison?

Response: The reviewer's point is well taken. However, we submit that it is a difficult task to undertake a comprehensive comparison unless a more detailed 3D model is used. In satellite data analysis, we used column/layer AOD and RH averaged between 100-440 hPa (or CAPE, U200) as proxies for aerosol loading related to ice clouds and overall available water amount at the upper atmosphere, respectively. However, the cloud parcel model only tracks the aerosol number concentration and water vapor within a single air parcel. It is clear that a direct and quantitative comparison between satellite observations and model results requires developing a 3-D atmospheric model and analysis, a difficult task for further investigation in the future.

Although the indices are not exactly the same, we submit that the simulated dependency of R_{ei} on aerosols could be used to qualitatively interpret the observed relationships, because the indices used in satellite analysis (AOD and RH averaged between 100-440 hPa) and parcel model (aerosol number concentration and water vapor mixing ratio) are closely correlated with each other, and that the meteorological parameters and aerosol concentration ranges used in the simulations are representative of typical in-situ ice clouds.

We have included these discussions in the revised manuscript. (Page 16, Line 32 to Page 17, Line 12)

References

Platnick S., King M. D., Meyer K. G., Wind G., Amarasinghe N., Marchant B., et al. MODIS cloud optical properties: User guide for the Collection 6 Level-2 MOD06/MYD06 product and associated Level-3 Datasets. 2015.

Reviewer 2

General Comments:

This referee agrees with the authors that this may be the first paper that studies the impact of aerosol concentration on cirrus cloud microphysics (through ice effective radius Rei in this case). The satellite observations appear valuable to our efforts to understand cirrus cloud-aerosol-radiation interactions, and should ultimately be published in ACP. However, the observations are interpreted narrowly, and much greater scope for interpretation should be provided. Alternate interpretations of the satellite retrievals have been provided under "Major Comments".

While the observations may contribute to our understanding of cirrus cloud-aerosol interactions, this may not be true for the cirrus cloud modeling work presented, as indicated below. It is recommended that Sect. 3.4 be dropped from the paper unless the concerns listed below can be adequately addressed. That is, the cloud model should predict cloud properties that are representative of in situ cirrus clouds, and the conditions assumed should also be representative. These modeling results are also irrelevant to anvil cirrus clouds, for the reasons stated in (14) below. The paper is well written and organized, with high quality figures. The observational methodology appears appropriate for this task; the other referee appears to be an expert in this area. The amount of supplementary material appears appropriate.

Response: We thank the Reviewer for constructive comments and suggestions. We have followed them carefully in revising the manuscript.

In particular, we have interpreted satellite observations more broadly (see our responses to the reviewer's 5th – 13rd major comments). We have also substantially improved the model simulations for application to in-situ ice clouds and clarified that the modeling results are not applicable to convection-generated ice clouds (see our responses to the reviewer's 14th – 16th major comments).

Below is a point-by-point response.

Major Comments:

1) Page 7, line 24: At what RHi do the deposition INP activate?

Response: Thank you. We have added the following sentence in the text. (Page 7, Line 19-22)

"The deposition nucleation on externally mixed dust (deposition INP) and immersion nucleation of coated dust (immersion INP) are parameterized following the work of Kuebbeler et al. (2014); the critical ice supersaturation ratios are 10% (T ≤ 220 K) or 20% (T > 220 K) for the former, and 30% for the latter."

2) Section 3: To gain confidence in the reported retrievals of Rei, these Rei retrievals could be compared against another Rei retrieval method reported in the literature. A global analysis of Rei is reported in Hong and Liu (J. Climate, 2015), based on CloudSat-CALIPSO measurements using the "DARDAR" method (a different method than used in this study). Although Hong and Liu do not relate Rei to aerosols, Rei is related to temperature, altitude and cloud optical depth, often as a function of latitude zone and season. Please make some comparisons, as direct as possible, between Hong and Liu Rei values and those reported in this paper.

Response: Thank you. Stein et al. (2011) has systematically compared the DARDAR R_{ei} retrievals with the MODIS data, as shown in Fig. R1. The default DARDAR retrievals of R_{ei} (denoted by VarCloud-OA, left panel) are mostly larger than MODIS's values. This discrepancy is partly induced by different assumptions of ice crystal habit (shape) in these two products. When the DARDAR retrievals are adjusted to mimic the MODIS assumption of ice crystal habit (VarCloud-BR, right panel), the joint distribution of individual R_{ei} retrievals has its peak close to the ratio of 1 between the two products, indicating a much better agreement. Nevertheless, the overall shape of the distributions indicates that the MODIS retrievals mostly lie between 10 and 50 μm, while both DARDAR products regularly retrieve R_{ei} above 60 μm. Hong and Liu (2015) reveals that the large R_{ei} values in DARDAR retrievals are predominantly associated with large cloud optical thickness (> 3.0, particularly > 20). In this study, however, we focus on ice-only clouds (mostly cirrus clouds), which typically have an optical thickness less than 5.0 (see Fig. 2 in the main text). For this reason, the agreement in R_{ei} between MODIS and DARDAR could be better for the type of cloud used in our analysis.

We have added the discussions above in the revised manuscript, citing Hong and Liu (2015) and Stein et al. (2011). (Page 4, Line 4-17)

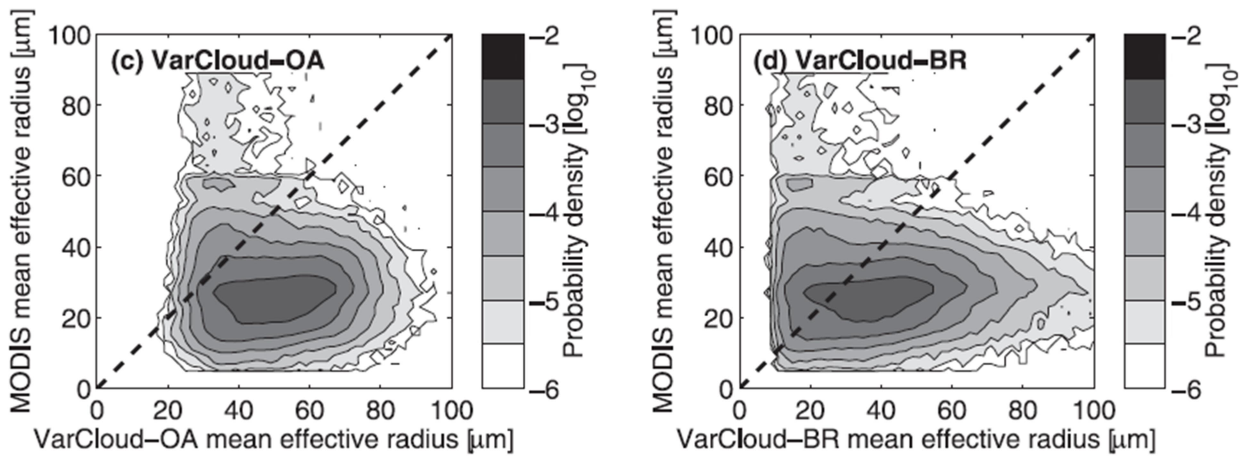

Figure R1. A comparison between the MODIS retrievals of R_{ei} and two DARDAR retrievals: left – the default DARDAR retrieval, denoted by VarCloud-OA; right – an adjusted DARDAR retrieval to mimic the MODIS assumption of ice crystal habit, denoted by VarCloud-BR. Data are from October 2008. Dashed lines in the figures indicate the 1:1 ratio. This figure is adapted from Stein et al. (2011). ©American Meteorological Society. Used with permission.

3) Section 3.1: The error bars in Fig. 1 and elsewhere denote standard errors ($\sigma/\sqrt{N}$) where σ is the standard deviation and N is the sample number. This makes the relationships difficult to interpret since we do not know what N is. Please use only σ for the error bars so the reader can better evaluate these relationships.

Response: Thank you. We submit that both standard error and standard deviation are widely used, but with different focuses. Standard deviation describes how spread out a set of measurements is, while standard error indicates how accurate our estimate of the mean is likely to be (McDonald, 2014). There is a probability of 68.3% that the population (true) mean would be within one standard error of the sample mean, and a probability of 95.4% to be within two standard errors (McDonald, 2014).

In this study, R_{ei} is affected not only by aerosol loading, but also a number of confounding factors such as meteorology, altitude, ice water content, etc. Some of these factors (e.g., meteorological conditions) may exert even larger effects on R_{ei} than aerosols. If standard deviations are plotted, we may not gain an idea whether changes in aerosol loading would induce significant changes in mean R_{ei}. However, the usage of standard errors could highlight the aerosol effects, because the population (true) mean for a given aerosol bin would very likely (with a 68.3% probability) fall within the error bars. Moreover, if the 95% confidence intervals (1.96 × standard error) of R_{ei} for two aerosol bins do not overlap, we would be sure that mean R_{ei} for these two aerosol bins are significantly different at the 0.05 level (McDonald, 2014). For these reasons, we submit that the standard error, which has been adopted by many observational studies on aerosol-cloud interactions (e.g., Jiang et al., 2011; Su et al., 2011; Koren et al., 2010; Li et al., 2011; Wang et al., 2015), appears to be suitable in our study. Additionally, we have specified the total number of samples used in each figure in the revised figure captions.

4) Page 9, line 14: Higher RH and CAPE imply that an air parcel will experience a longer time period exceeding ice saturation (i.e. longer time for supersaturation development, increasing the odds of exceeding the RHi threshold for homogeneous ice nucleation (henceforth hom)). This point could be made more clear.

Response: This suggestion is well taken. We have added this point in the revised manuscript:

"Under moist conditions (high RH, high CAPE, or negative U200), an air parcel could experience longer time for supersaturation development, increasing the odds of exceeding the supersaturation threshold for homogeneous ice nucleation." (Page 10, Line 29-32)

5) Page 10, lines 3-11 (1st paragraph): The similar dependence of Rei on column AOD (for all aerosol) and column AOD for dust aerosol only is critical to this study, and supports the assumption that ice nuclei (henceforth IN) concentration increases with increasing column AOD. However, this correspondence has only been demonstrated for column AOD and not for layer AOD (where layer AOD corresponds to cirrus cloud levels). Dust is often confined below cirrus cloud levels, and a column AOD-dust AOD relationship does not imply that one exists for layer AOD. Please make this point here.

Response: We have conducted a similar analysis for in-situ ice clouds and layer AOD for which the results are illustrated in Fig. R2 below (Fig. 3 in the revised manuscript). Similar to column AOD, the dependences of R_{ei} on layer AOD for all aerosols (Fig. R2a-c) and for dust only (Fig. R2d-f) are also similar. Since specific components of dust aerosols have been known as effective INPs, the similar R_{ei}-layer AOD relations imply that INP concentrations are also positively correlated with layer AOD, and that the proposed mechanisms for water vapor modulation is applicable to in-situ ice clouds and layer AOD.

We have supplemented this analysis in the revised manuscript. (Fig. 3; Page 11, Line 16-21)

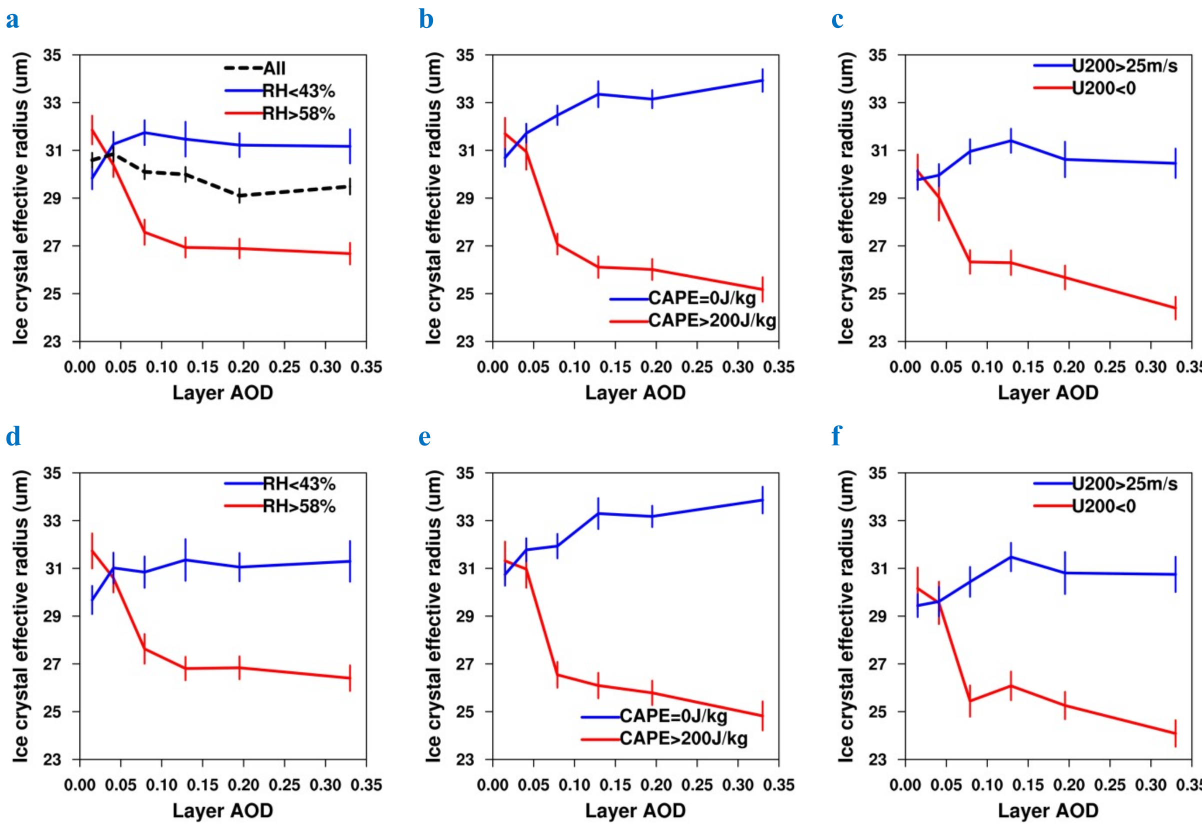

Figure R2. Changes in the R_{ei} of in-situ ice clouds with layer AOD for different ranges of (a) RH averaged between 100 hPa and 440 hPa, (b) CAPE, and (c) U200. (d-f) The same as (a-c) but for the profiles with dust aerosols only. The meteorological parameters are divided into 3 ranges containing similar numbers of data points, and the curves for the medium meteorological range are not shown. The error bars denote the standard errors ($\sigma/\sqrt{N}$) of the bin average, where σ is the standard deviation and N is the sample number. Note that we use AOD of the aerosol layers mixed with ice clouds rather than column AOD, since in-situ ice clouds are primarily affected by aerosols at the ice cloud height. The total number of samples used in this figure is 1.09×10^4.

6) Section 3.2: Rei is positively related to aerosol optical depth (AOD) under relatively dry conditions up to column AOD ~ 0.5 for convective ice clouds and up to ~ 0.13 AOD for in situ ice clouds. These Rei-AOD relationships in Fig. 1, 3 and 4 (for drier conditions) appear to result from competition effects between heterogeneous ice nucleation (henceforth het) and hom, where hom prevails at low AOD and het prevails at higher AOD. As het overtakes hom, Rei increases and ice crystal number concentration, Ni, decreases. This is known as the negative Twomey effect as first described by Kärcher and Lohmann (2003, JGR). Please explain this more thoroughly, citing this paper.

Response: Following the reviewer's comment, we have explained this process when describing both observational data and simulation results. Further, we have mentioned that this is known as the "negative Twomey effect" as first described by Karcher and Lohmann (2003). (Page 11, Line 1-7; Page 16, Line 9-19)

7) Section 3.2: Please state what percentage of the samples were convective vs. in situ.

Response: In response, the convective, in-situ, and other ice clouds account for 44.9%, 52.4%, and 2.7% for all ice cloud profiles. (Page 11, Line 25-27 in the revised manuscript)

8) Page 10, lines 32-33: For moist conditions in Fig. 3, this decrease in Rei with increasing AOD is no more than 2 microns, and the error bars show $\sigma/\sqrt{N}$, not σ (σ should be shown for meaningful interpretation). It is hard to argue that a significant decrease in Rei has occurred with increasing AOD.

Response: We have explained why we used standard error instead of standard deviation for the error bars in our response to the reviewer's 3rd comment. Based on the Student's t-test, the decreasing trends in R_{ei} under moist conditions (high RH, high CAPE, or negative U200) are all statistically significant at the 0.01 level. We have added the statistical test results in the revised manuscript. (Page 12, Line 21-24)

More discussion is needed here. As described in Kramer et al. (2016, ACP) and Luebke et al. (2017, ACP), anvil cirrus are a type of "liquid origin cirrus" where liquid cloud droplets contribute to the ice phase as they vertically advect into the cirrus zone (T < 235 K), freezing as they enter this zone. Ice particles from lower levels can also advect into the cirrus zone, especially for anvil cirrus. Cirrus ice from both sources can be viewed as "pre-existing ice" from a nucleation purview, which provides considerable ice surface area that suppresses the increase of ice supersaturation and prevents the RHi threshold for hom from being attained (Shi et al., 2015, ACP). For this reason, any new ice crystals formed in anvil cirrus are generally expected to form through het or ice crystal multiplication processes. This appears valid for both drier and moist conditions.

Lawson et al. (2015, JAS) combine laboratory measurements, in situ observations and modeling to show that Ni in tropical, convective cumulus clouds is dominated by ice multiplication, which may explain the relatively flat behavior of Rei for high CAPE, high RH and negative U. For such moist conditions, cloud droplets may grow to larger sizes required for ice multiplication. Ice crystals produced this way may be advected by the updraft into the anvil cirrus.

For zero CAPE, lower RH and positive U, ice multiplication may be less important (due to smaller droplet sizes), allowing Rei to increase with increasing AOD, characteristic of hom being overtaken by het (negative Twomey effect). For AOD > 0.4, Rei decreases in accord with het and increasing IN (positive Twomey effect expected when het prevails).

Please expand your discussion to include these points when discussing Fig. 3.

Response: The Reviewer's points are well-taken. The onset of ice multiplication may suppress or even prevent homogeneous nucleation to occur. In this situation, the rather weak decreasing trend in R_{ei} with increasing AOD can be explained, since ice multiplication is supposed to be stronger at the lower AOD that favors the formation of large cloud droplets required for ice multiplication (Lawson et al., 2015; Koenig, 1965, 1963).

We would like to submit that homogeneous nucleation might also play a role under moist conditions. To elucidate this point, we first need to clarify the meaning of "homogeneous nucleation" and "heterogeneous nucleation" with respect to convection-generated ice clouds in this study. The ice crystals in convection-generated ice clouds could be formed via several pathways. On one hand, ice crystals are produced by heterogeneous freezing of liquid droplets at temperatures larger than about –35 ^{o}C or possibly by homogeneous freezing of liquid droplets at about –35 ^{o}C (Kramer et al., 2016). The ice crystals are then lifted to the temperature range < –35 ^{o}C and are considered to be cirrus clouds (Kramer et al., 2016). On the other hand, an additional freezing of solution particles (in contrast to liquid droplets in the former case) may occur in the presence of "preexisting ice" if the updraft is sufficiently strong. The freezing mechanism is likely homogeneous nucleation, since INPs have already been consumed (Kramer et al., 2016). The reviewer points out that such additional freezing events are very difficult to occur and hence make less important contributions to ice crystal budget (Luebke et al., 2016), since the pre-existing ice suppresses supersaturation and prevents the threshold for homogeneous nucleation to take place (Shi et al., 2015). In this study, "homogeneous nucleation" refers to freezing of liquid droplets near the –35 ^{o}C isotherm as well as the freezing of solution particles below –35 ^{o}C. The former could be important for ice formation under moist conditions, because any liquid droplets would be homogeneously nucleated when they are lifted to the –35 ^{o}C isotherm. Evidence for homogeneous droplet freezing has been frequently observed in deep convective clouds and convection-generated cirrus clouds (Twohy and Poellot, 2005; Heymsfield et al., 2005; Rosenfeld and Woodley, 2000; Choi et al., 2010). In particular, liquid droplets are frequently observed to supercool to temperatures approaching –35 ^{o}C and even below, and at slightly colder temperature only ice is found, which serves as strong evidence for homogeneous droplet freezing (Rosenfeld and Woodley, 2000; Choi et al., 2010). Even if the occurrence frequency of homogeneous droplet freezing is low, its contribution to ice number concentration and R_{ei} may still be substantial in view of the fact that numerous ice crystals can be produced in a single homogeneous nucleation event. Under the situation dominated by homogeneous nucleation, the relatively flat response of R_{ei} to AOD (as compared to in-situ ice clouds) can also be explained as the mass fraction of homogeneously formed ice crystals is much smaller than that for in-situ ice clouds, as a result of substantial growth of heterogeneously formed ice crystals before reaching –35 ^{o}C isotherm. Whether the ice formation under moist conditions is dominated by homogeneous nucleation or ice multiplication is clearly dependent on environmental conditions such as updraft velocity, water vapor, cloud height and thickness, etc, a subject requiring further research.

We agree with the reviewer that, in dry conditions, ice multiplication may be less important due to smaller droplet sizes, therefore the increases in R_{ei} with increasing AOD are mainly attributable to the competition between heterogeneous and homogeneous nucleation in line with our original explanation. At a large AOD range (> 0.5), heterogeneous nucleation dominates and a further increase in aerosols would decrease R_{ei} due to the formation of more numerous and smaller ice crystals ("Twomey effect").

We have added the preceding discussions in the revised manuscript. (Page 12, Line 24-26; Page 12, Line 31 to Page 13, Line 22; Page 13, Line 32 to Page 14, Line 14)

9) Section 3.2, Fig. 4: For AOD < 0.10, the in situ cirrus Rei behavior for lower RH, zero CAPE and positive U could be interpreted as a negative Twomey effect with het overtaking hom due to increasing IN. For AOD > 0.10, if IN conc. is proportional to AOD, the trend should reverse with Rei decreasing with increasing AOD. This does not occur, and there is no evidence that the layer AOD is proportional to dust conc. As noted earlier. Thus it is possible that IN concentration is not tracking the layer AOD, and that IN conc. is relatively constant with AOD. This might explain the relatively flat Rei behavior for AOD > 0.10. Please point this out in the paper.

For the in situ cirrus Rei behavior for higher RH, higher CAPE and negative U (red curves), the interpretation given in this paper makes some sense. The freezing of solution droplets (i.e. hom) may be largely responsible for the decrease in Rei with increasing layer AOD.

Response: For AOD > 0.10 at lower RH, zero CAPE and positive U200, the trends in R_{ei} are not statistically significant judging from overlapping error bars. To evaluate the assumption that the INP concentration is not tracking layer AOD, which could explain these relative flat trends, we plot the relations between R_{ei} and layer AOD for dust only in Fig. R2d-f (shown in the response to the reviewer's 5th comment). We find that they are similar to the R_{ei}-layer AOD relations for all aerosol types (Fig. R2a-c). Since the INP concentrations certainly tracks AOD for dust aerosols, the above-mentioned assumption does not appear to account for the insignificant R_{ei} trend at AOD > 0.10. It appears likely that the layer AOD is not large enough, the environmental condition is not sufficiently dry, or the number of samples is not large enough to produce a significant decrease in R_{ei} with increasing layer AOD.

10) Page 11, lines 23-26: As stated in the paper, convective clouds vertically advect ice formed via het across the -35 C isotherm, but this "pre-existing ice" greatly suppresses supersaturations and generally prevents the RHi from reaching the RHi threshold for hom (Shi et al., 2015, ACP).

This may be true even for the "moist" convective conditions. Please include these points in the discussion (Sect. 3.2).

Response: The suggestion is well taken and we have included this point in the revised manuscript. (Page 13, Line 7-10)

11) Page 11, lines 29-32: Please state what percentage of sampled clouds were convective vs. in situ for each season. This is important for understanding the regional radiative implications of this work.

Response: The percentages of ice cloud profiles that are convection-generated type are 38.2%, 48.1%, 51.4%, and 39.1% in winter, spring, summer, and fall, respectively. The corresponding percentages for in-situ ice clouds are 57.0%, 49.6%, 47.0%, and 58.2%, respectively. We have included these descriptions in the revised manuscript. (Page 14, Line 32 to Page 15, Line 2)

12) Section 3.3, Fig. 5b: As noted under (8), ice multiplication can explain the relatively flat behavior of Rei during summer, and perhaps for spring and fall for AOD > 0.4. During winter, CAPE is much lower (see Fig. 5e), suggesting ice multiplication is less important here and Rei decreases for AOD > 0.4 in accord with het and increasing IN. For AOD < 0.4 during winter, spring and fall, Rei increases with increasing AOD, characteristic of hom being overtaken by het. (neg. Twomey effect). Please note this in the paper in regards to Fig. 5b.

Response: Following the reviewer's suggestion, we have included the following descriptions in the revised manuscript. (Page 15, Line 5-11)

"For convection-generated ice clouds, in winter, spring and fall, R_{ei} generally increases when AOD < 0.5, characteristic of homogeneous nucleation being overtaken by heterogeneous nucleation, while R_{ei} decreases slightly when AOD > 0.5 in accordance with heterogeneous nucleation and increasing INP concentrations. In summer, R_{ei} shows a weak decreasing trend with AOD, which could be explained by the domination of homogeneous nucleation or ice multiplication as described in Section 3.2."

13) Section 3.3, Fig. 5c: The summer in situ cirrus Rei behavior could be interpreted as a Twomey effect resulting from het and increasing IN, where deep convection injects more IN into the upper troposphere, thus promoting het. The deep convection during summer promotes tropospheric mixing, making it more likely that IN concentrations at cirrus levels track the layer AOD. It could also be argued that the flat in situ behavior during other seasons could be an indication that IN concentration is not tracking the layer AOD, and that IN concentration is

relatively constant with AOD (otherwise, an initial increase in Rei should be followed by a decrease in Rei as AOD increases). The different Rei values could then be explained in terms of seasonal differences in IN concentration, with lowest IN concentration in winter and highest in summer. Please discuss these points in the paper.

Response: Summer is characterized by relatively moist conditions (high RH, high CAPE, negative U200), in which homogeneous nucleation prevails for in-situ ice clouds as supported by both satellite data analysis and cloud parcel modeling. The "Twomey effect" resulting from heterogeneous nucleation and increasing INP should primarily occur at the dry condition with a large aerosol loading (see the reviewer's 8^{th} and 12^{th} comments and our replies). In other seasons, the weak correlation of INP concentration and layer AOD may partly explain the relative flat behavior of R_{ei}. Another probable reason for the weak R_{ei} trends is that each season consists of varying meteorological conditions (Fig. 4d-f). As shown in Fig. 3d-f, the decreasing trends in R_{ei} under moist conditions are strong, while the increasing trends under dry conditions are relatively weak. Even if the occurrence frequency of dry conditions is large in a season, say winter, the integration of all meteorological conditions may still yield a relative flat R_{ei}-aerosol relationship. We have described the seasonal variations in R_{ei}-layer AOD relations and the possible reasons in the revised manuscript. (Page 15, Line 11-20)

14) Page 13, lines 11-14: These modeling results may not apply to anvil cirrus for the reasons stated in (8) and (10). That is, Ni and Rei in anvil cirrus may be dominated by het and ice multiplication processes. Pre-existing ice should suppress RHi, suppressing hom, making the modeling results irrelevant to anvil cirrus.

Response: Thank you. We have clarified this point in the revised manuscript. (Page 16, Line 22-31)

"The current cloud parcel model simulates the environmental conditions and physical processes for in-situ ice clouds. For convection-generated ice clouds, the competition between homogeneous and heterogeneous nucleation may explain the observed R_{ei}-aerosol relations especially at dry conditions; however, the formation of this ice cloud type involves additional complex physical processes. As described in Section 3.2, ice multiplication together with heterogeneous nucleation may play an important role and dominate the ice formation in moist conditions. Furthermore, ice crystals in convection-generated ice clouds are formed primarily by freezing of liquid droplets rather than nucleation on solution particles."

15) Page 13, lines 23-28: The modeled Rei values for in situ cirrus clouds are ~ 1/3 those retrieved in this study for such clouds (and are typically ~ 1/3 or less of those from aircraft sampling of in situ cirrus clouds; e.g. Mishra et al., 2014, JGR). For a 30 minute simulation time,

the predicted values appear unrealistic. Isometric ice crystals grown at -22 ℃ reach ~ 100 microns in size after 10 minutes (Takahashi et al., 1991, J. Meteor. Soc. Japan), and would be much larger had the growth times been extended to 30 minutes. While growth rates will be lower at cirrus cloud temperatures, and vapor competition effects can limit growth rates, 30 minutes of growth time should still produce Rei values typical of cirrus clouds, which typically range from 10 and 45 μm at cirrus cloud temperatures based on aircraft measurements (Mishra et al., 2014, JGR).

The small Rei values imply very high Ni (assuming typical IWCs). Please also plot Ni vs. aerosol number conc. and comment on the realism of the Ni and IWC values.

The text here states variable updraft velocities as a possible reason for the small Rei predicted, but Sect. 2.3 states that a constant updraft velocity (w) of 0.5 m/s is applied throughout the 30 minute simulation time. The parcel model here is simulating in situ cirrus clouds, and w = 0.5 m/s is very high and not representative for in situ cirrus clouds. Hom is most sensitive to the cooling rate or w, and this simulation strongly favors hom due to the high w assumed. Hom can partly explain the small Rei values, but only when hom dominates. It cannot explain the black curve in Fig. 6a where het dominates for aerosol conc. above 200 cm-3; Rei should be ~ 3 times larger here. To summarize, the simulation here is not representative of in situ cirrus clouds and thus should not be used to interpret the satellite measurements.

Response: We have substantially improved the model simulations to make them representative of in-situ ice clouds including consideration of vertical velocity fluctuations and water vapor exchanges with other air parcels.

We conduct two groups of numerical experiments with different available water amount for ice formation, denoted by initial water vapor mass mixing ratios (pv). Each group is comprised of 100 sub-groups with initial sulfate number concentrations increasing linearly from 5 cm^{-3} to 500 cm^{-3}. The concentration ratios of externally mixed dust (deposition INP), coated dust (immersion INP), and sulfate (not INP) are prescribed with values of 0.75:0.25:10000 for all experiments, since INPs represent only 1 in 10^3 to 10^6 of ambient particles (Fan et al., 2016). In each sub-group, we conduct 100 one-hour experiments driven by different vertical velocity spectra following the approach described by Shi and Liu (2016). The vertical air motions at a 10 s resolution were retrieved from Millimeter Wave Cloud Radar (MMCR) observations at a site located in the Southern Great Plains (SGP; 36.6°N, 97.5°W) for a 6 h period (Shi and Liu, 2016). For each of the 100 experiments, we randomly sample a 1 h time windows from the 6 h vertical velocity retrievals, subtract the arithmetical mean, and adjust the standard deviation to 0.25 m s^{-1}. The sampled vertical velocity spectra are subsequently added a constant large-scale updraft velocity of 0.02 m s^{-1} to drive the parcel model.

The model assumes that the air parcel has no mass or energy exchange with the environment except for sedimentation of ice crystals, which is not realistic. For example, the outburst of homogeneous nucleation in an air parcel can quickly exhaust supersaturation and take water vapor from surrounding parcels. To conceptually mimic this process, we have divided the 100 experiments within a sub-group into 10 combinations, each consisting of 10 experiments. It is assumed that the air parcels in the same combination can exchange water vapor and reach equilibrium. Consequently, the occurrence of homogeneous nucleation in one parcel will suppress the homogeneous nucleation in the connected parcels due to the depletion of water vapor.

Figure R3a,b shows the simulated changes in R_{ei}, ice crystal number concentration (N_i), and the fraction of ice crystal number produced by heterogeneous nucleation as a function of the total aerosol number concentration. The N_i for a given aerosol number concentration (i.e., a sub-group of experiments) is calculated using an arithmetical mean of the 100 experiments, while R_{ei} is calculated from mean N_i and mean ice volume. At moist condition (pv = 103 ppm), R_{ei} decreases with increasing aerosol concentration, attributed to the "Twomey effect" when homogeneous nucleation dominates. At dry condition (pv = 78 ppm), R_{ei} increases with small-to-moderate aerosol loading, indicative of homogeneous nucleation overtaken by heterogeneous nucleation, and decreases with further aerosol increase in accordance with heterogeneous nucleation and the "Twomey effect". More importantly, the simulated magnitude of R_{ei} has been close to satellite observations (Figs. 1 and 3 in the revised manuscript), mainly due to the consideration of variable vertical velocities and water vapor exchanges between parcels. The mean N_i (across 100 experiments in each sub-group) of 10 to 250 L^{-1} (Fig. R3b) and mean ice water content of 1 to 24 ppm (not shown) are within the range reported in Kramer et al. (2016) based on a series of aircraft measurements.

To evaluate the effect of the assumption concerning water vapor exchange, we have performed a group of similar sensitivity simulations, except that the water vapor exchanges between parcels are deactivated (Fig. R3c,d). When heterogeneous nucleation dominates (i.e., pv = 78 ppm, large aerosol loadings), the magnitude of R_{ei} is similar regardless of the treatment of water vapor exchange. However, when homogeneous nucleation plays an important role, the simulated R_{ei} without water vapor exchange (Fig. R3c) is much smaller than the baseline simulation (Fig. R3a). We also note that the simulated R_{ei} is larger than the value shown in our previous manuscript even if water vapor exchange is not accounted for (Fig. R3c), because fluctuated vertical velocity spectra are applied here, resulting in overall less frequent and weaker homogeneous nucleation as compared to a large constant vertical velocity of 0.5 m s^{-1} used in our original manuscript.

We have added the methods and results of the new model simulations into the revised manuscript. (Fig. 5; Page 8, Line 5-33; Page 15, Line 28 to Page 16, Line 21)

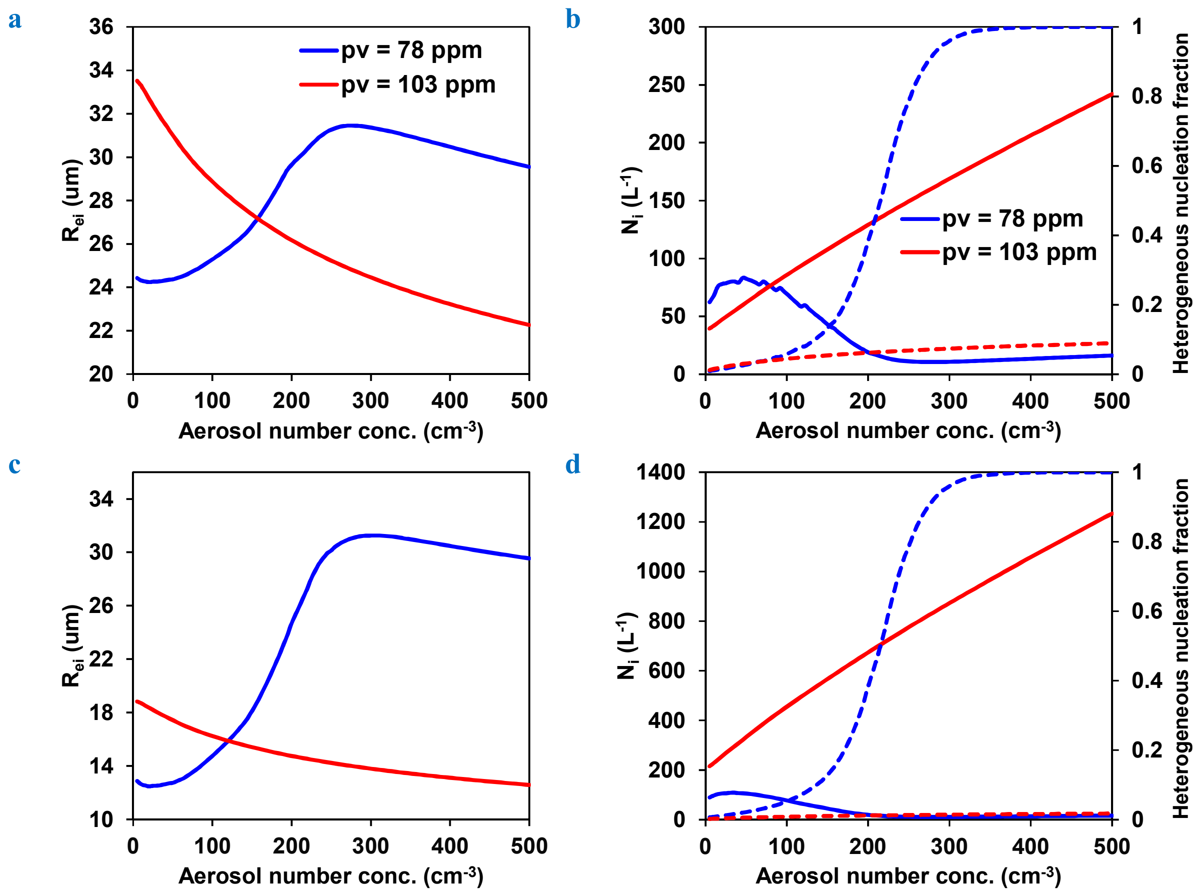

Figure R3. Simulated changes in (a) ice crystal effective radius (R_{ei}) and (b) ice crystal number concentration (N_i) and the fraction of ice crystal number produced by heterogeneous nucleation as a function of the total aerosol number concentration. (c-d) is the same as (a-b) except that the water vapor exchange between parcels is not accounted for. Simulations are conducted for two initial water vapor mass mixing ratios (pv) for ice formation. The ratios of externally mixed dust (deposition INP), coated dust (immersion INP), and sulfate (not INP) are prescribed with values of 0.75:0.25:10000 in all experiments.

16) Section 3.4, Fig. 6a: The beginning of the black curve is a manifestation of the "negative Twomy effect" (Karcher & Lohmann 2003, JGR) as hom is overtaken by het. The slope should become negative after aerosol conc. exceeds 200 cm-3 as increasing IN increases Ni, reducing Rei, but this does not happen. It is not clear why Rei does not decrease in this region.

Response: The decrease in R_{ei} in now shown in our new simulation results (blue line in Fig. R3a), as described in our response to the reviewer's 15th comment. This does not happen in the original simulations because the aerosol concentrations were not large enough to initiate a decline in R_{ei} in the context of a large constant vertical velocity of 0.5 m s^{-1}.

17) Section 3.4, Fig. 6b: As per my understanding, the initial water vapor mass mixing ratio (pv) determines the level of condensation and thus the portion of the 30 min. simulation time available for supersaturation development. In general, the INP concentrations assumed are sufficiently low to allow attainment of the hom RHi threshold, except for the pv = 38 ppm simulation which has less time for supersaturation development. If this is correct, then please make this clear in the text for greater clarity among the readership. In general, if this modeling section can be made relevant to in situ cirrus clouds, it needs to be expanded and explained better.

Response: We agree with the reviewer's explanation. For new simulations, the physical conditions are more complicated than the preceding description because the supersaturation is not always increasing under fluctuated vertical velocities. However, the general idea of "supersaturation development" is still applicable. We have revised the text as follows:

"With an adequate water vapor supply (pv = 103 ppm), the onset of deposition and immersion nucleation consumes only a small fraction of water vapor due to the small INP population. Considerable supersaturation remains. After further updraft movement, homogeneous nucleation is triggered and occurs spontaneously over a higher and narrow ice supersaturation range (140-160%). Therefore, homogeneous nucleation acts as the dominant ice formation pathway, as indicated by the very small number fraction (< 10%) of heterogeneously formed ice crystals, shown in Fig. 5b. With an inadequate water vapor supply (pv = 78 ppm), the occurrence of heterogeneous nucleation could consume a considerable fraction of water vapor such that the remaining supersaturation is quite low and would require extremely strong updraft to uphold the homogeneous nucleation threshold. When aerosol loading increases, homogeneous nucleation is gradually suppressed and reduced to a minimum." (Page 16, Line 1-16)

18) The following reference: "Ikawa, M., and Saito, K.: Description of a Non-hydrostatic Model Developed at the Forecast 38 Research Department of the MRI, Meteorological Research Institute, Tsukuba, Ibaraki, 39 Japan, 1991." is unconventional, and I wonder whether this is readily accessible. Can it be improved?

Response: We are sorry to report that this is the only reference we have found which describes the sedimentation scheme in detail. It is accessible to the public at http://www.mri-jma.go.jp/Publish/Technical/DATA/VOL_28/28_en.html. We have added the URL to the reference list.

Minor Comments:

1) Page 4, line 26: This might be a good place to state that your samples are strictly single-layer ice clouds, instead of at the end of this paragraph.

Response: Done, thank you. (Page 5, Line 16-18)

2) Page 5, line 1: Does cloud type assignment depend exclusively on the way it is flagged?

Response: The profiles of deep convective clouds are identified exclusively based on the "cloud type" flag in CALIPSO products, whereas the ice cloud profiles are identified following the standard that the "cloud type" flag is "cirrus" or its layer base temperature is colder than –35 ^{o}C. (Page 5, Line 5-6, Line 22-24)

3) Page 9, lines 15-16: Please indicate that U is the zonal wind as opposed to the meridional wind, and that positive U implies westerly winds; negative U implies easterly winds.

Response: Done, thank you. (Page 10, Line 18-20)

4) Page 12, line 32: Poor sentence; fix grammar. Should say something like "formation of more numerous and smaller ice crystals."

Response: Done, thank you. (Page 16, Line 7-9)

5) Page 13, line 15: Suggest replacing "discrepant" with "different" here and elsewhere throughout the paper.

Response: Done, thank you.

References

Bailey, M. P., and Hallett, J.: A Comprehensive Habit Diagram for Atmospheric Ice Crystals: Confirmation from the Laboratory, AIRS II, and Other Field Studies, J Atmos Sci, 66, 2888-2899, 10.1175/2009jas2883.1, 2009.

Choi, Y. S., Lindzen, R. S., Ho, C. H., and Kim, J.: Space observations of cold-cloud phase change, P Natl Acad Sci USA, 107, 11211-11216, 10.1073/pnas.1006241107, 2010.

Fan, J. W., Wang, Y., Rosenfeld, D., and Liu, X. H.: Review of Aerosol–Cloud Interactions: Mechanisms, Significance, and Challenges, J Atmos Sci, 73, 4221-4252, 2016.

Heymsfield, A. J., Miloshevich, L. M., Schmitt, C., Bansemer, A., Twohy, C., Poellot, M. R., Fridlind, A., and Gerber, H.: Homogeneous ice nucleation in subtropical and tropical convection and its influence on cirrus anvil microphysics, J Atmos Sci, 62, 41-64, 10.1175/jas-3360.1, 2005.

Hong, Y. L., and Liu, G. S.: The Characteristics of Ice Cloud Properties Derived from CloudSat and CALIPSO Measurements, J Climate, 28, 3880-3901, 10.1175/jcli-d-14-00666.1, 2015.

Jiang, J. H., Su, H., Zhai, C., Massie, S. T., Schoeberl, M. R., Colarco, P. R., Platnick, S., Gu, Y., and Liou, K. N.: Influence of convection and aerosol pollution on ice cloud particle effective radius, Atmos Chem Phys, 11, 457-463, 10.5194/acp-11-457-2011, 2011.

Karcher, B., and Lohmann, U.: A parameterization of cirrus cloud formation: Heterogeneous freezing, J Geophys Res-Atmos, 108, 10.1029/2002jd003220, 2003.

Koenig, L. R.: The glaciating behavior of small cumulonimbus clouds, J Atmos Sci, 20, 29-47, 10.1175/1520-0469(1963)020<0029:tgbosc>2.0.co;2, 1963.

Koenig, L. R.: Drop freezing through drop breakup, J Atmos Sci, 22, 448-&, 10.1175/1520-0469(1965)022<0448:dftdb>2.0.co;2, 1965.

Koren, I., Feingold, G., and Remer, L. A.: The invigoration of deep convective clouds over the Atlantic: aerosol effect, meteorology or retrieval artifact?, Atmos Chem Phys, 10, 8855–8872, doi:10.5194/acp-10-8855-2010, 2010.

Kramer, M., Rolf, C., Luebke, A., Afchine, A., Spelten, N., Costa, A., Meyer, J., Zoger, M., Smith, J., Herman, R. L., Buchholz, B., Ebert, V., Baumgardner, D., Borrmann, S., Klingebiel, M., and Avallone, L.: A microphysics guide to cirrus clouds - Part 1: Cirrus types, Atmos Chem Phys, 16, 3463-3483, 10.5194/acp-16-3463-2016, 2016.

Kuebbeler, M., Lohmann, U., Hendricks, J., and Karcher, B.: Dust ice nuclei effects on cirrus clouds, Atmos Chem Phys, 14, 3027-3046, 10.5194/acp-14-3027-2014, 2014.

Lawson, R. P., Baker, B., Pilson, B., and Mo, Q. X.: In situ observations of the microphysical properties of wave, cirrus, and anvil clouds. Part II: Cirrus clouds, J Atmos Sci, 63, 3186-3203, 10.1175/jas3803.1, 2006.

Lawson, R. P., Woods, S., and Morrison, H.: The Microphysics of Ice and Precipitation Development in Tropical Cumulus Clouds, J Atmos Sci, 72, 2429-2445, 10.1175/jas-d-14-0274.1, 2015.

Li, Z. Q., Niu, F., Fan, J. W., Liu, Y. G., Rosenfeld, D., and Ding, Y. N.: Long-term impacts of aerosols on the vertical development of clouds and precipitation, Nat Geosci, 4, 888-894, 10.1038/ngeo1313, 2011.

Luebke, A. E., Afchine, A., Costa, A., Grooss, J. U., Meyer, J., Rolf, C., Spelten, N., Avallone, L. M., Baumgardner, D., and Kramer, M.: The origin of midlatitude ice clouds and the resulting influence on their microphysical properties, Atmos Chem Phys, 16, 5793-5809, 10.5194/acp-16-5793-2016, 2016.

Lynch, D. K., Sassen, K., Starr, D., and Stephens, G.: Cirrus, Oxford University Press, New York, U.S.A., 2002.

McDonald, J. H.: Handbook of Biological Statistics (3rd ed.), Sparky House Publishing, Baltimore, Maryland, 2014.

Platnick, S., King, M. D., and Meyer, K. G.: MODIS cloud optical properties: user guide for the collection 6 level-2 MOD06/MYD06 product and associated level-3 datasets: https://modis-images.gsfc.nasa.gov/_docs/C6MOD06OPUserGuide.pdf, 2015.

Rosenfeld, D., and Woodley, W. L.: Deep convective clouds with sustained supercooled liquid water down to-37.5 degrees C, Nature, 405, 440-442, 10.1038/35013030, 2000.

Shi, X., Liu, X., and Zhang, K.: Effects of pre-existing ice crystals on cirrus clouds and comparison between different ice nucleation parameterizations with the Community Atmosphere Model (CAM5), Atmos Chem Phys, 15, 1503-1520, 10.5194/acp-15-1503-2015, 2015.

Shi, X., and Liu, X.: Effect of cloud-scale vertical velocity on the contribution of homogeneous nucleation to cirrus formation and radiative forcing, Geophys Res Lett, 43, 6588-6595, 10.1002/2016GL069531, 2016.

Stein, T. H. M., Delanoe, J., and Hogan, R. J.: A Comparison among Four Different Retrieval Methods for Ice-Cloud Properties Using Data from CloudSat, CALIPSO, and MODIS, J Appl Meteorol Clim, 50, 1952-1969, 10.1175/2011jamc2646.1, 2011.

Su, H., Jiang, J. H., Lu, X. H., Penner, J. E., Read, W. G., Massie, S., Schoeberl, M. R., Colarco, P., Livesey, N. J., and Santee, M. L.: Observed Increase of TTL Temperature and Water Vapor in Polluted Clouds over Asia, J Climate, 24, 2728-2736, 10.1175/2010JCLI3749.1, 2011.

Twohy, C. H., and Poellot, M. R.: Chemical characteristics of ice residual nuclei in anvil cirrus clouds: evidence for homogeneous and heterogeneous ice formation, Atmos Chem Phys, 5, 2289-2297, 2005.

Wang, F., Guo, J. P., Zhang, J. H., Huang, J. F., Min, M., Chen, T. M., Liu, H., Deng, M. J., and Li, X. W.: Multi-sensor quantification of aerosol-induced variability in warm clouds over eastern China, Atmos Environ, 113, 1-9, 10.1016/j.atmosenv.2015.04.063, 2015.

Impact of aerosols on ice crystal size

Bin Zhao[1], Kuo-Nan Liou[1], Yu Gu[1], Jonathan H. Jiang[2], Qinbin Li[1], Rong Fu[1], Lei Huang[1,2], Xiaohong Liu[3], Xiangjun Shi[3], Hui Su[2], and Cenlin He[1]

[1] Joint Institute for Regional Earth System Science and Engineering and Department of Atmospheric and Oceanic Sciences, University of California, Los Angeles, California 90095, USA.

[2] Jet propulsion Laboratory, California Institute of Technology, Pasadena, California 91109, USA.

[3] Department of Atmospheric Science, University of Wyoming, Laramie, Wyoming 82071, USA.

Correspondence to: Bin Zhao (zhaob1206@ucla.edu) and Yu Gu (gu@atmos.ucla.edu)

Abstract.

The interactions between aerosols and ice clouds represent one of the largest uncertainties in global radiative forcing from pre-industrial time to the present. In particular, the impact of aerosols on ice crystal effective radius (R_{ei}), which is a key parameter determining ice clouds' net radiative effect, is highly uncertain due to limited and conflicting observational evidence. Here we investigate the effects of aerosols on R_{ei} under different meteorological conditions using 9-year satellite observations. We find that the responses of R_{ei} to aerosol loadings are modulated by water vapor amount in conjunction with several other meteorological parameters. While there is a significant negative correlation between R_{ei} and aerosol loading in moist conditions, consistent with the "Twomey effect" for liquid clouds, a strong positive correlation between the two occurs in dry conditions. Simulations based on a cloud parcel model suggest that water vapor modulates the relative importance of different ice nucleation modes, leading to the opposite aerosol impacts between moist and dry conditions. When ice clouds are decomposed into those generated from deep convection and formed in-situ, the water vapor modulation remains in effect for both ice cloud types, although the sensitivities of R_{ei} to aerosols differ noticeably between them due to distinct formation mechanisms. The water vapor modulation can largely explain the difference in the responses of R_{ei} to aerosol

loadings in various seasons. A proper representation of the water vapor modulation is essential for an accurate estimate of aerosol-cloud radiative forcing produced by ice clouds.

1 Introduction

Aerosols are known to interact with clouds and hence affect Earth's radiative balance, which represents the largest uncertainty in global radiative forcing from pre-industrial time to the present (IPCC, 2013). The interactions between aerosols and liquid as well as mixed-phase clouds have been extensively studied (Rosenfeld et al., 2014; Seinfeld et al., 2016; Zhao et al., 2017b), however, much less attention has been paid to ice clouds, among which cirrus clouds are globally distributed and present at all latitudes and seasons with a global cloud cover of about 30% (Wylie et al., 1994; Wylie et al., 2005). Ice clouds, formed with various types of aerosols serving as ice nucleating particles (INPs) (Murray et al., 2012; Hoose and Moehler, 2012), act as a major modulator of global radiation budget and hence climatic parameters (e.g., temperature and precipitation) by reflecting solar radiation back to space (solar albedo effect, cooling) and by absorbing and re-emitting long-wave terrestrial radiation (greenhouse effect, warming); the balance between the two is dependent on ice cloud properties, particularly ice crystal size (Liou, 2005; Waliser et al., 2009; Fu and Liou, 1993). Limited estimates (IPCC, 2013; Liu et al., 2009; Fan et al., 2016) have shown that the global aerosol-cloud radiative forcing produced by ice clouds can be very significant but highly uncertain, ranging from –0.67 W m^{-2} to 0.70 W m^{-2}. For reference purposes, the best estimate of global aerosol-cloud radiative forcing produced by all cloud types is –0.45 W m^{-2} (90% confidence interval [–1.2, 0 W/m^2]) according to the Intergovernmental Panel on Climate Change (IPCC) (Fig. TS.6 in IPCC, 2013).

The substantial uncertainty in aerosol-ice cloud radiative forcing arises largely from a poor understanding of the aerosol effects on ice cloud properties, in particular ice crystal effective radius (R_{ei}), a key parameter determining ice clouds' net radiative effect (Fu and Liou, 1993). Very limited observational studies (Jiang et al., 2008; Jiang et al., 2011; Su et al., 2011; Chylek et al., 2006; Massie et al., 2007) have investigated the response of R_{ei} to aerosol loadings. Most of them (Jiang et al., 2008; Jiang et al., 2011; Su et al., 2011) found that polluted clouds involved smaller R_{ei} than clean clouds, in agreement with the classical "Twomey effect" for liquid clouds (Twomey, 1977), which states that more aerosols can result in more and smaller cloud droplets and hence larger cloud albedo. In contrast, a couple of studies over the Indian Ocean (Chylek et al., 2006; Massie et al., 2007) reported that R_{ei} is roughly unchanged (Massie et al., 2007) or larger (Chylek et al., 2006) during more polluted episodes. It has been shown that increased aerosols (and thus INPs) lead to enhanced heterogeneous nucleation, which is associated with larger and fewer ice crystals as compared to the homogeneous nucleation counterpart (DeMott et al., 2010; Chylek et al., 2006). However, the reasons for disagreement among various studies, and the controlling factors for different aerosol indirect effects are yet to be explored, therefore the sign and magnitude of the overall aerosol effects remain in question.

With the objective to resolve the substantial uncertainty, we systematically investigate the effects of aerosols on R_{ei} of two types of ice clouds under different meteorological conditions using 9-year continuous satellite observations from 2007 to 2015. The study region is East Asia and its surrounding areas (15º-55º N, 70º-135º E; Fig. S1), where aerosol loadings can range from small to extremely large values in different locations and time periods (Wang et al., 2017).

2 Data and Methods

2.1 Sources of observational data

We obtain collocated aerosol/cloud measurements primarily from MODIS (Moderate Resolution Imaging Spectroradiometer) onboard the Aqua satellite, and CALIPSO (Cloud-Aerosol Lidar and Infrared Pathfinder Satellite Observations), as summarized in Table S1.

We acquire aerosol optical depth (AOD) retrievals at 550 nm from the level 2 MODIS aerosol product (MYD04, Collection 6) at a resolution of 10 km × 10 km. The accuracy of AOD (denoted by τ) retrievals has been estimated to be about ±(0.05 + 0.15τ) over land and ±(0.03 + 0.05τ) over ocean (Levy et al., 2010; Remer et al., 2005). Similarly, we obtain cloud effective radius (equivalent to R_{ei} in the case of ice phase) and cloud phase determined by the "cloud optical property" algorithm from the level 2 MODIS cloud product (MYD06, Collection 6) at a 1 km × 1 km resolution (Platnick et al., 2015). The MYD06 product provides an estimate of the uncertainty in R_{ei} for each pixel, which takes into account a variety of error sources including 1) instrument calibration, 2) atmospheric corrections, 3) surface spectral reflectance, and 4) forward radiative transfer model, e.g., the size distribution assumption (Platnick et al., 2015). The pixel-level R_{ei} uncertainties for the samples used in this study are 6.41% ± 4.97% (standard deviation). In the subsequent analysis (Section 3.1-3.3) we use mean R_{ei} within certain AOD bins and the uncertainties are smaller than those for individual pixels. Also, we focus on R_{ei} changes in response to aerosol loading instead of absolute R_{ei} values. For these reasons, the R_{ei} uncertainty ranges are much smaller than the magnitude of R_{ei} trends depicted in this study (see Figs. 1 and 3). We note that the current uncertainty evaluation has not considered the assumptions of ice crystal habit (shape), which will be discussed in Section 3.4. Stein et al. (2011) compared the MODIS R_{ei} data with the "DARDAR" retrieval product (Delanoe and Hogan, 2008, 2010) based on CloudSat and CALIPSO measurements. The default DARDAR retrievals of R_{ei} are mostly larger than MODIS's values, which is partly attributable to different assumptions of ice crystal habit in these two products. When the DARDAR retrievals are adjusted to mimic the MODIS assumption of ice crystal habit, the joint distribution of individual R_{ei} retrievals has its peak close to the ratio of 1 between the two products, indicating a much better agreement (Stein et al., 2011). Nevertheless, the overall shape of the distributions indicates that the MODIS retrievals mostly lie between 10 and 50 μm, while both DARDAR products regularly retrieve R_{ei} above 60 μm. Hong and Liu (2015) reveals that the large R_{ei} values in DARDAR retrievals are predominantly associated with large cloud optical thickness (> 3.0, particularly > 20). In this study, however, we focus on ice-only clouds (mostly cirrus clouds), which typically have an optical thickness less than 5.0 (see Fig. 2). For this reason, the agreement in R_{ei} between MODIS and DARDAR could be better for the type of cloud used in our analysis.

The CALIPSO satellite flies behind Aqua by about 75 seconds and carries CALIOP (Cloud-Aerosol Lidar with Orthogonal Polarization), a dual-wavelength near-nadir polarization lidar (Winker et al., 2007). CALIOP has the capability to determine the global vertical distribution of aerosols and clouds. In this study, we make use of the CALIPSO level 2 merged aerosol and cloud layer product (05kmMLay, version 4.10) with an along-track resolution of 5 km and a high vertical resolution of 30-60 m below 20.2 km. The variables we employ for the investigation include aerosol/cloud layer numbers, layer base temperature, layer top/base height, layer aerosol/cloud optical depth, feature classification flags (containing the flags of "cloud type" and "aerosol type"), and two quality control (QC) flags named the cloud aerosol discrimination (CAD) score, and extinction QC (Atmospheric Science Data Center, 2012).

To examine the impact of meteorological conditions on aerosol-R_{ei} relations, we also obtain vertically-resolved pressure, relative humidity (RH), and temperature from the CALIPSO aerosol profile product (05kmAPro, version 4.10), and middle cloud layer temperature (T_{mid}) from the CALIPSO 05kmMLay product (version 4.10). The other meteorological parameters (see Table S1) are collected from the NCEP's Final Analysis reanalysis data (ds083.2), which are produced at a 1º × 1º resolution every six hours. Since Aqua and CALIPSO satellites overpass the study areas between 5:00-8:00 UTC, the ds083.2 datasets at 6:00 UTC are utilized.

2.2 Processing of observational data

In the analysis, we identify a CALIPSO profile layer at 5 km resolution as ice cloud when its "cloud type" is "cirrus" or its layer base temperature is colder than –35 ^{o}C. Previous studies (Mace et al., 2001; Mace et al., 2006; Kramer et al., 2016) have distinguished two major types of ice clouds characterized by distinct formation mechanisms: ice clouds generated from deep convection (convection-generated ice clouds) and those generated in-situ due to updraft caused by frontal systems, gravity waves, or orographic waves (in-situ ice clouds). Considering that the impact of aerosols could differ according to formation processes, we separate these two ice cloud types using CALIPSO data and a similar approach to that developed by Riihimaki and McFarlane (2010). First, we group ice cloud profiles at 5 km resolution into objects using the criteria that neighboring ice cloud profiles must vertically overlap (the base of the higher cloud layer is lower than the top of the lower cloud layer) and be separated by no more than 1 profiles horizontally (i.e., distance ⩽ 5 km). Only single-layer ice cloud objects with valid QA flags (20 ⩽ CAD score ⩽ 100, Extinction QC = 0/1) are accepted in this study. We subsequently classify ice cloud objects into three types, i.e., convection-generated, in-situ, and other ice clouds, according to their connection to other clouds. The criteria to determine whether two clouds are connected are consistent with that used to group ice cloud objects, i.e., the neighboring profiles must vertically overlap and horizontally seperated by no more than 5 km. Convection-generated ice clouds consist of ice cloud objects that are connected to larger clouds that include deep convective cloud profiles (i.e., the "cloud type" flag is "deep convection"). An ice cloud object is classified as in-situ if at least 95% of a cloud consists of a single ice cloud object which is at least 25 km (i.e., 5 profiles) in the horizontal direction, and none of the remaining profiles are deep convection type. The remaining ice cloud objects are catogorized as the "other" type. We should be cautious that the convection-generated and in-situ ice clouds may not be perfectly separated using the approach described above. For example, the in-situ ice clouds indentified here could include convectively-detrained objects that are no longer connected with their parent deep convection, and convectively-detrained objects whose parent deep convective clouds do not overlap with CALIPSO's track. The convection-generated ice clouds may also be contaminated by some in-situ formed ice cloud objects that happen to be spatially connected to deep convection. However, the classification scheme appears to be reasonable, as indicated by the distinct properties of the two ice cloud types shown in Section 3.2.

We then match collocated MODIS/Aqua and CALIPSO observations by averaging retrieved AOD and R_{ei} from MODIS level 2 products (MYD04 and MYD06) within 30 km and 5 km radii of each 5 km ice cloud profile from CALIPSO, respectively. The averaging is done to achieve near-simultaneous aerosol and cloud measurements, since AOD observations from MODIS are missing at cloudy conditions. As AOD variation has a large spatial length scale of 40-400 km (Anderson et al., 2003), it is averaged within a larger radius than that for R_{ei} to increase the number of data points with valid AOD observations. The average R_{ei} is calculated based on the pixels with "cloud phase" of ice. Apart from the column AOD, we also need to obtain AOD of the aerosol layers mixed with ice cloud layers, as in-situ ice clouds are primarily affected by aerosols at the ice cloud height. For this purpose, we use the CALIPSO 05kmMLay product to select the aerosol layers which have valid QA flags ($-100 \leqslant$ CAD score $\leqslant -20$, Extinction QC = 0/1; Huang et al., 2013) and are vertically less than 0.25 km away from the ice cloud layer following Costantino and Breon (2010). The AOD of these aerosol layers are averaged within a 30 km radius of ice cloud profiles. The meteorological parameters from the NCEP datasets (ds083.2) are matched to the CALIPSO resolution by determining which NCEP's grid contains a certain CALIPSO 5 km profile. Finally, we eliminate profiles with column AOD > 1.5 to reduce the potential effect of cloud contamination (Wang et al., 2015).

Convection-generated ice clouds are generated by convective updraft originating from lower troposphere and are therefore affected by aerosols at various altitudes, whereas in-situ ice clouds are primarily dependent on aerosols near the cloud height. For this reason, we use column AOD and layer AOD mixed with ice clouds as proxies for aerosols interacting with convection-generated and in-situ ice clouds, respectively. We also investigate the overall effect of aerosols on all types of ice clouds. In this case, column AOD is used as a proxy for aerosol loading affecting ice clouds following a number of previous studies (Jiang et al., 2011; Massie et al., 2007; Ou et al., 2009). The rationale is that the MODIS-detected AOD generally shows a close correlation to the MLS (Microwave Limb Sounder)-observed CO concentration in ice clouds (Jiang et al., 2008; Jiang et al., 2009), which in turn correlates well with the aerosol loading mixed with clouds in accordance with both aircraft measurements and atmospheric modeling (Jiang et al., 2009; Li et al., 2005; Clarke and Kapustin, 2010). After the preceding screening, about 2.73×10^4, 1.09×10^4, and 5.68×10^4 profiles are used to analyze the relationships between column/layer AOD and R_{ei} of convection-generated, in-situ, and all types of ice clouds. The available profiles for in-situ ice clouds are fewer because aerosols mixed with ice clouds are often optically thin or masked by clouds and hence may not be fully detected by CALIPSO.

2.3 Cloud parcel model simulation

To support the key findings (i.e., the water vapor modulation of R_{ei}-aerosol relations) from satellite observations and elucidate the underlying physical mechanisms, we perform model simulations using a cloud parcel model, which was originally developed by Shi and Liu (2016) and updated in this study to incorporate immersion nucleation. The model mimics formation and evolution of in-situ ice clouds in an adiabatically rising air parcel. The model's governing equations that describe the evolution of temperature, pressure, and mass mixing ratio, number concentration, and size of ice crystals can be found in Pruppacher and Klett (1997). The main microphysical processes considered include homogeneous nucleation and two modes of heterogeneous nucleation (deposition and immersion nucleation), depositional growth, sublimation, and sedimentation. The rate of homogeneous nucleation of supercooled sulfate droplets is calculated based on the water activity of sulfate solution (Shi and Liu, 2016). The dry sulfate aerosol is assumed to follow a lognormal size distribution with a geometric mean radius of 0.02 μm. The deposition nucleation on externally mixed dust (deposition INP) and immersion nucleation of coated dust (immersion INP) are parameterized following the work of Kuebbeler et al. (2014); the critical ice supersaturation ratios are 10% ($T \leq 220$ K) or 20% ($T > 220$ K) for the former, and 30% for the latter. Anthropogenic INPs are not included in the cloud parcel model following recent studies (Shi and Liu, 2016; Kuebbeler et al., 2014). This is because 1) ice nucleation experiments for black carbon show contradicting results (Hoose and Moehler, 2012), and 2) ice nucleation parameterizations for anthropogenic aerosol constituents other than black carbon have not been adequately developed under ice cloud conditions due to limited experimental data. Also, we find that the relationships between R_{ei} and loadings of dust aerosols are similar to those between R_{ei} and loadings of all aerosols (Section 3.1). As such, we argue that the general pattern of simulation results would remain unchanged if more INPs were incorporated. The accommodation coefficient of water vapor deposition on ice crystals is assumed to be 0.1 (Shi and Liu, 2016). The sedimentation velocity of ice crystals is parameterized following Ikawa and Saito (1991). The model neglects some ice microphysical processes such as aggregational growth of ice crystals. Although aggregational growth can affect the concentration and size of ice crystals, its effects should be relatively small in terms of the response of R_{ei} to aerosol loading since this process is not strongly dependent on aerosols.

We conduct two groups of numerical experiments with different available water amount for ice formation, denoted by initial water vapor mass mixing ratios (pv). Each group is comprised of 100 sub-groups with initial sulfate number concentrations increasing linearly from 5 cm^{-3} to 500 cm^{-3}. The concentration ratios of externally mixed dust (deposition INP), coated dust (immersion INP), and sulfate (not INP) are prescribed with values of 0.75:0.25:10000 for all experiments, since INPs represent only 1 in 10^3 to 10^6 of ambient particles (Fan et al., 2016). In each sub-group, we conduct 100 one-hour experiments driven by different vertical velocity spectra following the approach described by Shi and Liu (2016). The vertical air motions at a 10 s resolution were retrieved from Millimeter Wave Cloud Radar (MMCR) observations at a site located in the Southern Great Plains (SGP; 36.6°N, 97.5°W) for a 6 h period (Shi and Liu, 2016). For each of the 100 experiments, we randomly sample a 1 h time windows from the 6 h vertical velocity retrievals, subtract the arithmetical mean, and adjust the standard deviation to 0.25 m s^{-1}. The sampled vertical velocity spectra are subsequently added a constant large-scale updraft velocity of 0.02 m s^{-1} to drive the parcel model. The initial pressure and temperature for all experiments are set at 250 hPa and 220 K, respectively.

The model assumes that the air parcel has no mass or energy exchange with the environment except for sedimentation of ice crystals, which is not realistic. For example, the outburst of homogeneous nucleation in an air parcel can quickly exhaust supersaturation and take water vapor from surrounding parcels. To conceptually mimic this process, we have divided the 100 experiments within a sub-group into 10 combinations, each consisting of 10 experiments. It is assumed that the air parcels in the same combination can exchange water vapor and reach equilibrium. Consequently, the occurrence of homogeneous nucleation in one parcel will suppress the homogeneous nucleation in the connected parcels due to the depletion of water vapor.

The ice crystal number concentration (N_i) and R_{ei} at the end of the experiments are used to construct the aerosol-cloud relationships. The N_i for a given aerosol number concentration (i.e., a sub-group of experiments) is calculated using an arithmetical mean of the 100 experiments, while R_{ei} is calculated from mean N_i and mean ice volume.

3 Results and Discussion

3.1 Relationships between R_{ei} and aerosols modulated by meteorology

In this section we discuss the impact of aerosols on R_{ei}, with both ice cloud types lumped together, based on satellite data (Fig. 1). The aerosol effects on individual ice cloud types will be discussed in the next section. The dash line in Fig. 1a shows the overall changes in R_{ei} with AOD. R_{ei} generally increases with increasing AOD for moderate AOD range (< 0.5), and decreases slightly for higher AOD. This relationship is attributable to complex interactions between meteorological conditions and microphysical processes, which will be detailed below.

Having shown overall response of R_{ei} to AOD, we investigate whether the responses are similar under different meteorological conditions. We plot the R_{ei}-AOD relationships separately for different ranges of meteorological parameters, as shown in Fig. 1a-c and Fig. S2. Included in the analysis are most meteorological parameters that can potentially affect ice cloud formation and evolution, including the relative humidity averaged between 100 hPa and 440 hPa ($RH_{100\text{-}440hPa}$), convective available potential energy (CAPE) which is an indicator of convective strength, middle cloud layer temperature (T_{mid}), wind speed and direction at ice cloud height and at surface, vertical velocity below and at ice cloud height, and vertical wind shear. For some meteorological parameters, e.g., vertical wind shear and vertical velocity at 300/500 hPa, the curve shapes are similar for different meteorological ranges. However, for $RH_{100\text{-}440hPa}$, CAPE, and U-component of wind speed at 200 hPa (U200), the curve shapes vary significantly according to different ranges (Fig. 1a-c). As illustrated by $RH_{100\text{-}440hPa}$ and CAPE, R_{ei} decreases significantly with increasing AOD for high $RH_{100\text{-}440hPa}$ (> 65%) or CAPE (> 500 J/kg) following the rule of "Twomey effect". In contrast, for low $RH_{100\text{-}440hPa}$ (< 45%) or CAPE (0 J/kg), R_{ei} generally increases sharply with AOD; an exception is that at a large AOD range (> 0.5), a further increase in AOD could decrease R_{ei} slightly. To the best of our knowledge, the strong dependency of R_{ei}-AOD relationships on meteorological conditions for ice clouds has been demonstrated for the first time.

These correlations, however, may not be necessarily attributed to aerosols. It is theoretically possible that certain meteorological parameters lead to simultaneous changes in both AOD and ice cloud properties and produce a correlation between these two parameters. To rule out this possibility, we examine the responses of AOD to the above-mentioned meteorological parameters (Fig. S3) and find that AOD does not serve as proxy for them since it varies by less than 0.2 in response to variation in any meteorological parameter. Furthermore, we bin observed R_{ei} according to $RH_{100\text{-}440hPa}$, CAPE, and U200, for different ranges of AOD (Fig. 1d-f). Using $RH_{100\text{-}440hPa}$ as an example, a larger AOD corresponds to smaller R_{ei} for a given $RH_{100\text{-}440hPa}$ within the larger $RH_{100\text{-}440hPa}$ range, whereas an increase in AOD enlarges R_{ei} for a given $RH_{100\text{-}440hPa}$ within the smaller $RH_{100\text{-}440hPa}$ range. Similar results are found for CAPE and U200 (Fig. 1d-f), demonstrating the role of aerosols in altering R_{ei} under the same meteorological conditions. Moreover, the cloud contamination in AOD retrieval (Kaufman et al., 2005) or aerosol contamination in cloud retrieval (Brennan et al., 2005) is not likely to lead to observed R_{ei}-AOD correlations, because the retrieval biases cannot explain the opposite correlations under different meteorological conditions. Therefore, we conclude that both the positive and negative correlations between AOD and R_{ei} are primarily attributed to the aerosol effect. This causality is also supported by numerical simulations using a cloud parcel model to be described in Section 3.4. Furthermore, we find that the three meteorological parameters which pose the strongest impact on R_{ei}-AOD relationships ($RH_{100\text{-}440hPa}$, CAPE, and U200) are closely correlated with each other, with correlation coefficients between each two exceeding ±0.5 and p-value less than 0.01 (Table S2). In fact, all these three parameters are closely related to the amount of water vapor available for ice cloud formation. It is obvious that $RH_{100\text{-}440hPa}$ is an indicator of water vapor amount. CAPE represents convective strength and hence water vapor lifted to ice cloud heights; U200 is the zonal wind at 200 hPa as opposed to the meridional wind, and denotes the origin of air mass such as moist Pacific Ocean (negative U200, easterly wind) or dry inland continent (positive U200, westerly wind). Therefore, water vapor amount is likely a key factor which modulates the observed impact of aerosols on R_{ei}.

The proposed mechanism for the water vapor modulation is that different water vapor amount substantially alters the relative significance of different ice nucleation modes, thereby resulting in different R_{ei}-AOD relationships. Specifically, ice crystals form via two primary pathways: homogeneous nucleation of liquid cloud droplets (or supercooled solution particles) below about −35 °C, and heterogeneous nucleation triggered by INPs (IPCC, 2013; DeMott et al., 2010). INPs possess surface properties favorable to lowering the ice supersaturation ratio required for freezing (IPCC, 2013; DeMott et al., 2010), therefore the onset of heterogeneous nucleation is generally easier and earlier in rising air parcels. Under moist conditions (high $RH_{100\text{-}440hPa}$, high CAPE, or negative U200), an air parcel could experience longer time for supersaturation development, increasing the odds of exceeding the supersaturation threshold for homogeneous ice nucleation. Therefore, homogeneous nucleation dominates in this case, and more aerosols could give rise to more numerous and smaller ice crystals, which is in connection with the "Twomey effect" for liquid clouds. Under dry conditions, however, the earlier onset of heterogeneous nucleation can strongly compete with and possibly prevent homogeneous nucleation involving more abundant liquid droplets or solution particles (IPCC, 2013; DeMott et al., 2010). Therefore, more aerosols (and hence more INPs) are expected to lead to a higher fraction of ice crystals produced by heterogeneous nucleation comprising of fewer and larger ice crystals. This is known as "negative Twomey effect" as first described by Karcher and Lohmann (2003). At very large AOD range (> 0.5), heteorogeneous nucleation dominates and a further increase in aerosols would decrease R_{ei} due to the formation of more smaller ice crystals. These proposed mechanisms will be supported and elaborated on using model simulations in Section 3.4.

Here an inherent assumption is that INP concentration is roughly proportional to, or at least positively correlated with AOD. Considering that INPs only account for a small fraction of ambient aerosols, we may not take this assumption for granted. Here we plot the R_{ei}-AOD relations using only the cases in which the "aerosol type" (a flag contained in the feature classification flags of CALIPSO) is dust (Fig. 1g-i), and find that the water modulation effect is very similar to the preceding results (i.e., Fig. 1a-c). In addition to column AOD, we also find similar dependences of R_{ei} on layer AOD (mixed with in-situ ice clouds) for all aerosols and for dust only (see Fig. 3d-i). Since specific components of dust aerosols have been known as effective INPs (Murray et al., 2012; Hoose and Moehler, 2012), the similar R_{ei}-AOD relations of dust and of all aerosols to some extent support the proposed mechanisms for water vapor modulation.

3.2 R_{ei}-aerosol relationships for two types of ice clouds

Considering that distinct formation mechanisms of convection-generated and in-situ ice clouds may lead to different aerosol effects, we distinguish these two ice cloud types based on their connection to deep convection (Section 2.2). In the study region, the convection-generated, in-situ, and other ice clouds account for 44.9%, 52.4%, and 2.7% of all ice cloud profiles, respectively. Figure 2 illustrates the accumulative probability distribution of cloud thickness, cloud optical thickness (COT), and R_{ei} of the two ice cloud types. The cloud thickness and COT of convection-generated ice clouds are remarkably larger than those of in-situ ice clouds, because more water is transported to upper troposphere in the formation process of the former type, consistent with numerous aircraft measurement results (e.g., Kramer et al., 2016; Luebke et al., 2016; Muhlbauer et al., 2014). The R_{ei} of convection-generated ice clouds is slightly larger than that of in-situ ice clouds, which has also been reported in a number of aircraft campaigns (Luebke et al., 2016; Kramer et al., 2016). The larger R_{ei} in convection-generated ice clouds is attributed to larger water amount and the fact that they are produced by convection emerging from lower altitude. Below the –35 ^{o}C isotherm, ice crystals stem only from heterogeneous nucleation, which tends to produce larger ice crystals compared to the homogeneous nucleation counterpart (Luebke et al., 2016).

Figures 3 shows the impact of aerosols on R_{ei} under different meteorological conditions for convection-generated and in-situ ice clouds, respectively. As described in Section 2.2, we use column AOD and layer AOD mixed with ice clouds as proxies of aerosols interacting with convection-generated and in-situ ice clouds, respectively. The most impressive feature from these figures is that the meteorology modulation remains in effect for either of the two ice cloud types, such that R_{ei} generally decreases with AOD under high $RH_{100\text{-}440hPa}$/high CAPE/negative U200 conditions, whereas the reverse is true under low $RH_{100\text{-}440hPa}$/low CAPE/positive U200 conditions. Similar to the Section 3.1, we also demonstrate that the R_{ei}-aerosol relationships are primarily attributed to the aerosol effect by illustrating role of aerosols in altering R_{ei} under the nearly constant meteorological conditions (Fig. S4). For example, a larger AOD is associated with a smaller R_{ei} for a given $RH_{100\text{-}440hPa}$ within the larger $RH_{100\text{-}440hPa}$ range, while an increase in AOD leads to a larger R_{ei} for a given $RH_{100\text{-}440hPa}$ within the smaller $RH_{100\text{-}440hPa}$ range. These results illustrate that the meterology modulation of aerosol effects on R_{ei} is valid regardless of ice cloud formation machanisms.

A closer look at Fig. 3 shows that there exist noted differences between the R_{ei}-aerosol relationships for the two ice cloud types. For convection-generated ice clouds, a weak negative correlation (but still statistically significant at the 0.01 level) between R_{ei} and AOD is found under moist conditions, while a strong positive correlation is found under dry conditions. Note that at a large AOD range (> 0.5) under dry conditions, a further increase in AOD could slightly reduce R_{ei} because of the "Twomey effect" when heterogeneous nucleation prevails. For in-situ ice clouds, however, weaker positive and stronger negative correlations are shown under dry and moist conditions, respectively. As a result, overall R_{ei} slightly increases with aerosol loading for convection-generated ice clouds, but slightly dcreases for in-situ clouds.

These differences are again linked to the distinct formation mechanisms of the two ice cloud types. As the formation mechanism of convection-generated ice clouds is quite complex, we first briefly review major pathways of ice crystal formation in convection-generated clouds. On one hand, ice crystals are produced by heterogeneous freezing of liquid droplets at temperatures larger than about –35 ^{o}C or possibly by homogeneous freezing of liquid droplets at about –35 ^{o}C (Kramer et al., 2016). The ice crystals are then lifted to the temperature range < –35 ^{o}C and are considered to be ice clouds (Kramer et al., 2016). On the other hand, an additional freezing of solution particles (in contrast to liquid droplets in the former case) may occur in the presence of "preexisting ice" if the updraft is sufficiently strong. The freezing mechanism is likely homogeneous nucleation, since INPs have already been consumed (Kramer et al., 2016). Such additional freezing events are very difficult to occur and hence make less important contributions to ice crystal budget (Luebke et al., 2016), since the pre-existing ice suppresses supersaturation and prevents the threshold for homogeneous nucleation to take place (Shi et al., 2015). In this study, "homogeneous nucleation" refers to freezing of liquid droplets near the –35 ^{o}C isotherm as well as the freezing of solution particles below –35 ^{o}C. The former could be important for ice formation, because any liquid droplets would be homogeneously nucleated when they are lifted to the –35 ^{o}C isotherm. Evidence for homogeneous droplet freezing has been frequently observed in deep convective clouds and convection-generated cirrus clouds (Twohy and Poellot, 2005; Heymsfield et al., 2005; Rosenfeld and Woodley, 2000; Choi et al., 2010). In particular, liquid droplets are frequently observed to supercool to temperatures approaching –35 ^{o}C and even below, and at slightly colder temperature only ice is found, which serves as strong evidence for homogeneous droplet freezing (Rosenfeld and Woodley, 2000; Choi et al., 2010). Even if the occurrence frequency of homogeneous droplet freezing is low, its contribution to ice number concentration and R_{ei} may still be substantial in view of the fact that numerous ice crystals can be produced in a single homogeneous nucleation event.

Obviously, convection-generated ice clouds are influenced by aerosols at various heights, which presumably contain much more INPs than the thin upper tropospheric aerosol layers in the case of in-situ ice clouds. In addition, the heterogeneously formed ice crystals in convective clouds are able to grow before being lifted to –35 ^{o}C isotherm where homogeneous nucleation bursts, giving rise to a larger difference between the ice crystal sizes produced by heterogeneous and homogeneous nucleation as compared to in-situ ice clouds. For these reasons, under dry conditions, the increase in R_{ei} with aerosol loading, which is due to the transition from homogeneous-dominated to heterogeneous-dominated regimes, would be much more pronounced for convection-generated ice clouds.

At moist conditions, homogeneous nucleation could dominate for both ice cloud types as described in Section 3.1, but the mass fraction of homogeneously formed ice crystals is smaller for convection-generated ice clouds than that for in-situ ice clouds, leading to a weaker decline in R_{ei} with aerosols. Alternatively, for convection-generated ice clouds, ice multiplication, a microphysical process in which collision between ice particles and large supercooled droplets rapidly produces many secondary ice particles in strong updrafts (Lawson et al., 2015; Koenig, 1965, 1963), could also play a remarkable role in ice formation. Its role could be important only under moist conditions where cloud droplets may grow to large sizes required for ice multiplication (Lawson et al., 2015; Koenig, 1965, 1963). The onset of ice multiplication may suppress or even prevent homogeneous nucleation to occur. In the situation dominated by ice multiplication, the relatively flat response of R_{ei} to AOD in case of convection-generated ice clouds can also be explained, since ice multiplication is supposed to be stronger at the lower AOD which favors the formation of large cloud droplets. Whether the ice formation under moist conditions is dominated by homogeneous nucleation or ice multiplication is clearly dependent on environmental conditions such as updraft velocity, water vapor, cloud height and thickness, etc, a subject requiring further research.

3.3 Seasonal variations in R_{ei}-aerosol relationships

Furthermore, we find that the meteorological modulation can largely explain differences in R_{ei}-AOD relationships as a function of season. Figure 4a shows that the R_{ei}-AOD relationships are dramatically different associated with season, such that R_{ei} decreases significantly with increasing AOD in summer (June, July, and August), while R_{ei} increases rapidly in winter (December, January, and February). Figure 4d-f illustrate the probability distribution functions (PDFs) of $RH_{100\text{-}440hPa}$, CAPE, and U200 in different seasons (the area under any PDF equals 1.0). The overlapping area of PDFs in summer and winter represents the degree of difference in meteorological conditions between these two seasons. We find that meteorological conditions are significantly distinct in summer and winter in terms of $RH_{100\text{-}440hPa}$, CAPE, and U200, as indicated by relatively small overlapping areas (<0.6) for these three parameters. The $RH_{100\text{-}440hPa}$ and CAPE tend to be higher and U200 tends to be more negative in summer. Moreover, the shapes of R_{ei}-AOD curves in summer and winter highly resemble those under high-$RH_{100\text{-}440hPa}$/high-CAPE/negative-U200 and low-$RH_{100\text{-}440hPa}$/low-CAPE/positive-U200 conditions, respectively (see Fig. 1a-c), which demonstrates that the discrepancy in meteorological conditions between winter and summer can, to a large extent, explain the distinct R_{ei}-AOD relationships in these two seasons.

With regard to different ice cloud types, the percentages of ice cloud profiles that are convection-generated type are 38.2%, 48.1%, 51.4%, and 39.1% in winter, spring, summer, and fall, respectively. The corresponding percentages for in-situ ice clouds are 57.0%, 49.6%, 47.0%, and 58.2%, respectively. Fig. 4b-c show that, for both ice cloud types, the R_{ei}-aerosol curves in summer and winter are largely similar to those under moist and dry conditons (Fig. 3), indicating that the seasonal variations in R_{ei}-aerosol relations for both ice cloud types are largely attributable to the meteorology modulation. For convection-generated ice clouds, in winter, spring and fall, R_{ei} generally increases when AOD < 0.5, characteristic of homogeneous nucleation being overtaken by heterogeneous nucleation, while R_{ei} decreases slightly when AOD > 0.5 in accordance with heterogeneous nucleation and increasing INP concentrations. In summer, R_{ei} shows a weak decreasing trend with AOD, which could be explained by the domination of homogeneous nucleation or ice multiplication as described in Section 3.2. For in-situ ice clouds, a sharp decline in R_{ei} with AOD is observed in summer, attributed to the "Twomey effect" when homogeneous nucleation prevails. The trends in other seasons are rather weak (although an increase is noticed in winter at low layer AOD). A probable reason is that each season consists of varying meteorological conditions (Fig. 4d-f). As shown in Fig. 3d-f, the decreasing trends in R_{ei} under moist conditions are strong, while the increasing trends under dry conditions are relatively weak. Even if the occurrence frequency of dry conditions is large in a season, say winter, the integration of all meteorological conditions may still yield a relative flat R_{ei}-aerosol relationship. Another possible reason is that the correlation of INP concentration and layer AOD could be weak in some physical conditions.

3.4 Modeling support for the water vapor modulation

We have shown that the R_{ei}-aerosol relationships are modulated by meteorological conditions, particularly water vapor amount. To support the observed relationships and our proposed physical mechanisms, we perform model simulations as described in Section 2.3 and summarize the results in Fig. 5.

Figure. 5a reveals that the simulated patterns of R_{ei}-aerosol relationships under different water vapor amount agree fairly well with the corresponding observed patterns (Fig. 1a-c). Specifically, with an adequate water vapor supply (pv = 103 ppm), R_{ei} decreases significantly with aerosol concentrations ("Twomey effect"). Under a dry condition (pv = 78 ppm), R_{ei} increases noticeably with small-to-moderate aerosol concentrations ("negative Twomey effect"), and decreases slightly with further aerosol increase. A deeper analysis of the simulation results supports our proposed mechanism (Section 3.1) that the competition between different ice nucleation modes is the key to explain the water vapor modulation.

With an adequate water vapor supply (pv = 103 ppm), the onset of deposition and immersion nucleation consumes only a small fraction of water vapor due to the small INP population. Considerable supersaturation remains. After further updraft movement, homogeneous nucleation is triggered and occurs spontaneously over a higher and narrow ice supersaturation range (140-160%). Therefore, homogeneous nucleation acts as the dominant ice formation pathway, as indicated by the very small number fraction (< 10%) of heterogeneously formed ice crystals, shown in Fig. 5b. In this case, more aerosols are associated with the formation of more numerous and smaller ice crystals, consistent with the simulation results of Liu and Penner (2005). With an inadequate water vapor supply (pv = 78 ppm), Fig. 5b reveals that the number fraction of heterogeneously formed ice crystals increases dramatically from < 1% to ~95% when aerosol number concentrations increase from 5 cm^{-3} to ~300 cm^{-3} (the INP number concentrations increase proportionally). Obviously, the occurrence of heterogeneous nucleation could consume a considerable fraction of water vapor such that the remaining supersaturation is quite low and would require extremely strong updraft to uphold the homogeneous nucleation threshold. When aerosol loading increases, homogeneous nucleation is gradually suppressed and reduced to a minimum. Since the outburst of homogeneous nucleation generally produces more ice crystals at smaller size compared with the heterogeneous counterpart, an increasing fraction of heterogeneous nucleation would result in fewer ice crystals with larger average size ("negative Twomey effect"). At larger aerosol loading (> 300 cm^{-3}), a further aerosol increase slightly reduces R_{ei} in accordance with heterogeneous nucleation and the "Twomey effect".

The current cloud parcel model simulates the environmental conditions and physical processes for in-situ ice clouds. For convection-generated ice clouds, the competition between homogeneous and heterogeneous nucleation may explain the observed R_{ei}-aerosol relations especially at dry conditions; however, the formation of this ice cloud type involves additional complex physical processes. As described in Section 3.2, ice multiplication together with heterogeneous nucleation may play an important role and dominate the ice formation in moist conditions. Furthermore, ice crystals in convection-generated ice clouds are formed primarily by freezing of liquid droplets rather than nucleation on solution particles. The simulation of the aerosol impact on convection-generated ice clouds calls for more sophisticated models and future investigations.

As a simplified model, the simulation results of the cloud parcel model may not be quantitatively compard with the observational data. In satellite data analysis, we used column/layer AOD and $RH_{100\text{-}440hPa}$ (or CAPE, U200) as proxies for aerosol loading related to ice clouds and overall available water amount at the upper atmosphere, respectively. However, the cloud parcel model only tracks the aerosol number concentration and water vapor within a single air parcel. It is clear that a direct and quantitative comparison between satellite observations and model results requires developing a 3-D atmospheric model and analysis, a difficult task for further investigation in the future. Although the indices are not exactly the same, we submit that the simulated dependency of R_{ei} on aerosols could be used to qualitatively interpret the observed relationships, because the indices used in satellite analysis (AOD and $RH_{100\text{-}440hPa}$) and parcel model (aerosol number concentration and water vapor mixing ratio) are closely correlated with each other, and that the meteorological parameters and aerosol concentration ranges used in the simulations are representative of typical in-situ ice clouds.

Finally, a factor that could potentially induce changes in satellite-retrieved R_{ei} but has not been considered is the habit of ice crystals. Based on previous studies (Bailey and Hallett, 2009; Lawson et al., 2006; Lynch et al., 2002), the habit of ice crystals is dependent on a number of factors, among which the most important one is temperature, followed by ice supersaturation ratio. In this study we focus on R_{ei} changes with aerosol loading, for which temperature does not appear to have noticeable effect. For supersaturation ratio, the formation of ice crystals under moist conditions is dominated by homogeneous nucleation, therefore the ice supersaturation ratio surrounding ice crystals is usually very low and the ice habit is not likely to change significantly with aerosol loading. Under drier conditions, however, heterogeneous nucleation gradually takes over homogeneous nucleation with aerosol loading increase. Subsequently, the supersaturation ratio surrounding ice crystals would become higher, possibly leading to changes in ice crystal habit. Considering that a single habit (i.e., aggregated column) is assumed in Collection 6 MODIS retrieval algorithm (Platnick et al., 2015), ice habit changes could possibly induce changes in the satellite-retrieved R_{ei}. However, this retrieval bias should not change our major conclusion about the aerosol impact on ice crystal size, which has been supported by the cloud parcel modeling used in this study. The quantitative assessment of the impact of ice crystal habit on satellite retrievals of R_{ei} is a very complicated and difficult task that merits further study.

4 Conclusions and implications

In this study, we investigate the effects of aerosols on R_{ei} under different meteorological conditions using 9-year satellite observations. We find that the responses of R_{ei} to aerosol loadings are modulated by water vapor amount in conjunction with several other meteorological parameters, and vary from a significant negative correlation ("Twomey effect") to a strong positive correlation ("negative Twomey effect"). Simulations using a cloud parcel model indicate that the water vapor modulation works primarily by altering the relative importance of different ice nucleation modes. The water vapor modulation holds true for both convection-generated and in-situ ice clouds, though the sensitivities of R_{ei} to aerosols differ noticeably between these two ice cloud types due to distinct formation mechanisms. The water vapor modulation can largely explain the different responses of R_{ei} to aerosol loadings in various seasons.

R_{ei} is a key parameter determining the relative significance of the solar albedo (cooling) effect and the infrared greenhouse (warming) effect of ice clouds; the variation of R_{ei} could change the sign of ice clouds' net radiative effect (Fu and Liou, 1993). Aerosols have strong and intricate effects on R_{ei} through their indirect effect. We provide the first and direct evidence that the competition between the "Twomey effect" and "negative Twomey effect" is controlled by certain meteorological parameters, primarily water vapor amount. Consequently, the first aerosol indirect forcing, defined as the radiative forcing due to aerosol-induced changes in R_{ei} under a constant ice water content (IPCC, 2013; Penner et al., 2011), would change from positive to negative between high and low RH ranges, implying that the water vapor modulation could play an important role in determining the sign, magnitude, and probably seasonal and regional variations of aerosol-ice cloud radiative forcings. An adequate and accurate representation of this modulation in climate models will undoubtedly induce changes in the magnitude and sign of the current estimate of aerosol-ice cloud radiative forcing. Finally, although this study focuses on East Asia, we anticipate that the present findings might be generalized to other regions as well in view of the fact that the aerosol loadings in East Asia usually span a larger range than other regions (Zhao et al., 2017a) and that the aerosol effects on ice cloud properties are particularly pronounced at low and moderate aerosol loadings (Figs. 1, 3, 4).

Acknowledgements

Research work contained in this paper has been supported by NSF EAGER Grant AGS-1523296, NSF Grant AGS-1701526, and NASA ROSES ACMAP and CCST grants. We also acknowledge the support of the Joint Institute for Regional Earth System Science and

Engineering at University of California, Los Angeles and the Jet Propulsion Laboratory, California Institute of Technology, under contract with NASA.

References

Anderson, T. L., Charlson, R. J., Winker, D. M., Ogren, J. A., and Holmen, K.: Mesoscale variations of tropospheric aerosols, J Atmos Sci, 60, 119-136, Doi 10.1175/1520-0469(2003)060<0119:Mvota>2.0.Co;2, 2003.

Atmospheric Science Data Center: CALIPSO Quality Statements Lidar Level 2 Cloud and Aerosol Layer Products Version Releases: 3.01, 3.02: https://eosweb.larc.nasa.gov/PRODOCS/calipso/Quality_Summaries/CALIOP_L2LayerProducts_3.01.html, access: October 1, 2016, 2012.

Bailey, M. P., and Hallett, J.: A Comprehensive Habit Diagram for Atmospheric Ice Crystals: Confirmation from the Laboratory, AIRS II, and Other Field Studies, J Atmos Sci, 66, 2888-2899, 10.1175/2009jas2883.1, 2009.

Brennan, J. I., Kaufman, Y. J., Koren, I., and Li, R. R.: Aerosol-cloud interaction-misclassification of MODIS clouds in heavy aerosol, IEEE T Geosci Remote, 43, 911-915, 10.1109/Tgrs.2005.844662, 2005.

Choi, Y. S., Lindzen, R. S., Ho, C. H., and Kim, J.: Space observations of cold-cloud phase change, P Natl Acad Sci USA, 107, 11211-11216, 10.1073/pnas.1006241107, 2010.

Chylek, P., Dubey, M. K., Lohmann, U., Ramanathan, V., Kaufman, Y. J., Lesins, G., Hudson, J., Altmann, G., and Olsen, S.: Aerosol indirect effect over the Indian Ocean, Geophys Res Lett, 33, L06806, DOI 10.1029/2005gl025397, 2006.

Clarke, A., and Kapustin, V.: Hemispheric aerosol vertical profiles: Anthropogenic impacts on optical depth and cloud nuclei (vol 329, pg 1488, 2010), Science, 330, 1047-1047, 2010.

Costantino, L., and Breon, F. M.: Analysis of aerosol-cloud interaction from multi-sensor satellite observations, Geophys Res Lett, 37, L11801, DOI 10.1029/2009gl041828, 2010.

Delanoe, J., and Hogan, R. J.: A variational scheme for retrieving ice cloud properties from combined radar, lidar, and infrared radiometer, J Geophys Res-Atmos, 113, 10.1029/2007jd009000, 2008.

Delanoe, J., and Hogan, R. J.: Combined CloudSat-CALIPSO-MODIS retrievals of the properties of ice clouds, J Geophys Res-Atmos, 115, 10.1029/2009jd012346, 2010.

DeMott, P. J., Prenni, A. J., Liu, X., Kreidenweis, S. M., Petters, M. D., Twohy, C. H., Richardson, M. S., Eidhammer, T., and Rogers, D. C.: Predicting global atmospheric ice nuclei distributions and their impacts on climate, P Natl Acad Sci USA, 107, 11217-11222, 10.1073/pnas.0910818107, 2010.

Fan, J. W., Wang, Y., Rosenfeld, D., and Liu, X. H.: Review of Aerosol–Cloud Interactions: Mechanisms, Significance, and Challenges, J Atmos Sci, 73, 4221-4252, 2016.

Fu, Q., and Liou, K. N.: Parameterization of the Radiative Properties of Cirrus Clouds, J Atmos Sci, 50, 2008-2025, Doi 10.1175/1520-0469(1993)050<2008:Potrpo>2.0.Co;2, 1993.

Heymsfield, A. J., Miloshevich, L. M., Schmitt, C., Bansemer, A., Twohy, C., Poellot, M. R., Fridlind, A., and Gerber, H.: Homogeneous ice nucleation in subtropical and tropical convection and its influence on cirrus anvil microphysics, J Atmos Sci, 62, 41-64, 10.1175/jas-3360.1, 2005.

Hong, Y. L., and Liu, G. S.: The Characteristics of Ice Cloud Properties Derived from CloudSat and CALIPSO Measurements, J Climate, 28, 3880-3901, 10.1175/jcli-d-14-00666.1, 2015.

Hoose, C., and Moehler, O.: Heterogeneous ice nucleation on atmospheric aerosols: a review of results from laboratory experiments, Atmos Chem Phys, 12, 9817-9854, 10.5194/acp-12-9817-2012, 2012.

Huang, L., Jiang, J. H., Tackett, J. L., Su, H., and Fu, R.: Seasonal and diurnal variations of aerosol extinction profile and type distribution from CALIPSO 5-year observations, J Geophys Res-Atmos, 118, 4572-4596, 10.1002/jgrd.50407, 2013.

Ikawa, M., and Saito, K.: Description of a Non-hydrostatic Model Developed at the Forecast Research Department of the MRI, available at http://www.mri-jma.go.jp/Publish/Technical/DATA/VOL_28/28_en.html, Meteorological Research Institute, Tsukuba, Ibaraki, Japan, 1991.

IPCC: Climate Change 2013: The Physical Science Basis. Contribution of Working Group I to the Fifth Assessment Report of the Intergovernmental Panel on Climate Change, edited by: Stocker, T. F., Qin, D., Plattner, G.-K., Tignor, M., Allen, S. K., Boschung, J., Nauels, A., Xia, Y., Bex, V., and Midgley, P. M., Cambridge University Press, Cambridge, United Kingdom and New York, NY, USA, 1535 pp., 2013.

Jiang, J. H., Su, H., Schoeberl, M. R., Massie, S. T., Colarco, P., Platnick, S., and Livesey, N. J.: Clean and polluted clouds: Relationships among pollution, ice clouds, and precipitation in South America, Geophys Res Lett, 35, L14804, DOI 10.1029/2008gl034631, 2008.

Jiang, J. H., Su, H., Massie, S. T., Colarco, P. R., Schoeberl, M. R., and Platnick, S.: Aerosol-CO relationship and aerosol effect on ice cloud particle size: Analyses from Aura Microwave Limb Sounder and Aqua Moderate Resolution Imaging Spectroradiometer observations, J Geophys Res-Atmos, 114, D20207, DOI 10.1029/2009jd012421, 2009.

Jiang, J. H., Su, H., Zhai, C., Massie, S. T., Schoeberl, M. R., Colarco, P. R., Platnick, S., Gu, Y., and Liou, K. N.: Influence of convection and aerosol pollution on ice cloud particle effective radius, Atmos Chem Phys, 11, 457-463, 10.5194/acp-11-457-2011, 2011.

Karcher, B., and Lohmann, U.: A parameterization of cirrus cloud formation: Heterogeneous freezing, J Geophys Res-Atmos, 108, 10.1029/2002jd003220, 2003.

Kaufman, Y. J., Koren, I., Remer, L. A., Rosenfeld, D., and Rudich, Y.: The effect of smoke, dust, and pollution aerosol on shallow cloud development over the Atlantic Ocean, P Natl Acad Sci USA, 102, 11207-11212, 10.1073/pnas.0505191102, 2005.

Koenig, L. R.: The glaciating behavior of small cumulonimbus clouds, J Atmos Sci, 20, 29-47, 10.1175/1520-0469(1963)020<0029:tgbosc>2.0.co;2, 1963.

Koenig, L. R.: Drop freezing through drop breakup, J Atmos Sci, 22, 448-&, 10.1175/1520-0469(1965)022<0448:dftdb>2.0.co;2, 1965.

Kramer, M., Rolf, C., Luebke, A., Afchine, A., Spelten, N., Costa, A., Meyer, J., Zoger, M., Smith, J., Herman, R. L., Buchholz, B., Ebert, V., Baumgardner, D., Borrmann, S., Klingebiel, M., and Avallone, L.: A microphysics guide to cirrus clouds - Part 1: Cirrus types, Atmos Chem Phys, 16, 3463-3483, 10.5194/acp-16-3463-2016, 2016.

Kuebbeler, M., Lohmann, U., Hendricks, J., and Karcher, B.: Dust ice nuclei effects on cirrus clouds, Atmos Chem Phys, 14, 3027-3046, 10.5194/acp-14-3027-2014, 2014.

Lawson, R. P., Baker, B., Pilson, B., and Mo, Q. X.: In situ observations of the microphysical properties of wave, cirrus, and anvil clouds. Part II: Cirrus clouds, J Atmos Sci, 63, 3186-3203, 10.1175/jas3803.1, 2006.

Lawson, R. P., Woods, S., and Morrison, H.: The Microphysics of Ice and Precipitation Development in Tropical Cumulus Clouds, J Atmos Sci, 72, 2429-2445, 10.1175/jas-d-14-0274.1, 2015.

Levy, R. C., Remer, L. A., Kleidman, R. G., Mattoo, S., Ichoku, C., Kahn, R., and Eck, T. F.: Global evaluation of the Collection 5 MODIS dark-target aerosol products over land, Atmos Chem Phys, 10, 10399-10420, 10.5194/acp-10-10399-2010, 2010.

Li, Q. B., Jiang, J. H., Wu, D. L., Read, W. G., Livesey, N. J., Waters, J. W., Zhang, Y. S., Wang, B., Filipiak, M. J., Davis, C. P., Turquety, S., Wu, S. L., Park, R. J., Yantosca, R.

M., and Jacob, D. J.: Convective outflow of South Asian pollution: A global CTM simulation compared with EOS MLS observations, Geophys Res Lett, 32, L14826, DOI 10.1029/2005gl022762, 2005.

Liou, K. N.: Cirrus clouds and climate in McGraw-Hill Yearbook of Science and Technology, McGraw-Hill Professional, New York, U.S.A., 2005.

Liu, X. H., and Penner, J. E.: Ice nucleation parameterization for global models, Meteorologische Zeitschrift, 14, 499-514, 10.1127/0941-2948/2005/0059, 2005.

Liu, X. H., Penner, J. E., and Wang, M. H.: Influence of anthropogenic sulfate and black carbon on upper tropospheric clouds in the NCAR CAM3 model coupled to the IMPACT global aerosol model, J Geophys Res-Atmos, 114, D03204, DOI 10.1029/2008jd010492, 2009.

Luebke, A. E., Afchine, A., Costa, A., Grooss, J. U., Meyer, J., Rolf, C., Spelten, N., Avallone, L. M., Baumgardner, D., and Kramer, M.: The origin of midlatitude ice clouds and the resulting influence on their microphysical properties, Atmos Chem Phys, 16, 5793-5809, 10.5194/acp-16-5793-2016, 2016.

Lynch, D. K., Sassen, K., Starr, D., and Stephens, G.: Cirrus, Oxford University Press, New York, U.S.A., 2002.

Mace, G. G., Clothiaux, E. E., and Ackerman, T. P.: The composite characteristics of cirrus clouds: Bulk properties revealed by one year of continuous cloud radar data, J Climate, 14, 2185-2203, 10.1175/1520-0442(2001)014<2185:tccocc>2.0.co;2, 2001.

Mace, G. G., Benson, S., and Vernon, E.: Cirrus clouds and the large-scale atmospheric state: Relationships revealed by six years of ground-based data, J Climate, 19, 3257-3278, 10.1175/jcli3786.1, 2006.

Massie, S. T., Heymsfield, A., Schmitt, C., Muller, D., and Seifert, P.: Aerosol indirect effects as a function of cloud top pressure, J Geophys Res-Atmos, 112, D06202, DOI 10.1029/2006jd007383, 2007.

Muhlbauer, A., Ackerman, T. P., Comstock, J. M., Diskin, G. S., Evans, S. M., Lawson, R. P., and Marchand, R. T.: Impact of large-scale dynamics on the microphysical properties of midlatitude cirrus, J Geophys Res-Atmos, 119, 3976-3996, 10.1002/2013jd020035, 2014.

Murray, B. J., O'Sullivan, D., Atkinson, J. D., and Webb, M. E.: Ice nucleation by particles immersed in supercooled cloud droplets, Chem Soc Rev, 41, 6519-6554, 10.1039/c2cs35200a, 2012.

Ou, S. S. C., Liou, K. N., Wang, X. J., Hansell, R., Lefevre, R., and Cocks, S.: Satellite remote sensing of dust aerosol indirect effects on ice cloud formation, Appl Optics, 48, 633-642, 10.1364/Ao.48.000633, 2009.

Penner, J. E., Xu, L., and Wang, M. H.: Satellite methods underestimate indirect climate forcing by aerosols, P Natl Acad Sci USA, 108, 13404-13408, 10.1073/pnas.1018526108, 2011.

Platnick, S., King, M. D., and Meyer, K. G.: MODIS cloud optical properties: user guide for the collection 6 level-2 MOD06/MYD06 product and associated level-3 datasets: https://modis-images.gsfc.nasa.gov/_docs/C6MOD06OPUserGuide.pdf, 2015.

Pruppacher, H. R., and Klett, J. D.: Microphysics of Cloud and Precipitation, Springer, New York, U.S.A., 1997.

Remer, L. A., Kaufman, Y. J., Tanre, D., Mattoo, S., Chu, D. A., Martins, J. V., Li, R. R., Ichoku, C., Levy, R. C., Kleidman, R. G., Eck, T. F., Vermote, E., and Holben, B. N.: The MODIS aerosol algorithm, products, and validation, J Atmos Sci, 62, 947-973, Doi 10.1175/Jas3385.1, 2005.

Riihimaki, L. D., and McFarlane, S. A.: Frequency and morphology of tropical tropopause layer cirrus from CALIPSO observations: Are isolated cirrus different from those connected to deep convection?, J Geophys Res-Atmos, 115, 10.1029/2009jd013133, 2010.

Rosenfeld, D., and Woodley, W. L.: Deep convective clouds with sustained supercooled liquid water down to-37.5 degrees C, Nature, 405, 440-442, 10.1038/35013030, 2000.

Rosenfeld, D., Andreae, M. O., Asmi, A., Chin, M., de Leeuw, G., Donovan, D. P., Kahn, R., Kinne, S., Kivekas, N., Kulmala, M., Lau, W., Schmidt, K. S., Suni, T., Wagner, T., Wild, M., and Quaas, J.: Global observations of aerosol-cloud-precipitation-climate interactions, Rev Geophys, 52, 750-808, 10.1002/2013RG000441, 2014.

Seinfeld, J. H., Bretherton, C., Carslaw, K. S., Coe, H., DeMott, P. J., Dunlea, E. J., Feingold, G., Ghan, S., Guenther, A. B., Kahn, R., Kraucunas, I., Kreidenweis, S. M., Molina, M. J., Nenes, A., Penner, J. E., Prather, K. A., Ramanathan, V., Ramaswamy, V., Rasch, P. J., Ravishankara, A. R., Rosenfeld, D., Stephens, G., and Wood, R.: Improving our fundamental understanding of the role of aerosol-cloud interactions in the climate system, P Natl Acad Sci USA, 113, 5781-5790, 10.1073/pnas.1514043113, 2016.

Shi, X., Liu, X., and Zhang, K.: Effects of pre-existing ice crystals on cirrus clouds and comparison between different ice nucleation parameterizations with the Community Atmosphere Model (CAM5), Atmos Chem Phys, 15, 1503-1520, 10.5194/acp-15-1503-2015, 2015.

Shi, X., and Liu, X.: Effect of cloud-scale vertical velocity on the contribution of homogeneous nucleation to cirrus formation and radiative forcing, Geophys Res Lett, 43, 6588-6595, 10.1002/2016GL069531, 2016.

Stein, T. H. M., Delanoe, J., and Hogan, R. J.: A Comparison among Four Different Retrieval Methods for Ice-Cloud Properties Using Data from CloudSat, CALIPSO, and MODIS, J Appl Meteorol Clim, 50, 1952-1969, 10.1175/2011jamc2646.1, 2011.

Su, H., Jiang, J. H., Lu, X. H., Penner, J. E., Read, W. G., Massie, S., Schoeberl, M. R., Colarco, P., Livesey, N. J., and Santee, M. L.: Observed Increase of TTL Temperature and Water Vapor in Polluted Clouds over Asia, J Climate, 24, 2728-2736, 10.1175/2010JCLI3749.1, 2011.

Twohy, C. H., and Poellot, M. R.: Chemical characteristics of ice residual nuclei in anvil cirrus clouds: evidence for homogeneous and heterogeneous ice formation, Atmos Chem Phys, 5, 2289-2297, 2005.

Twomey, S.: Influence of pollution on shortwave albedo of clouds, J Atmos Sci, 34, 1149-1152, 10.1175/1520-0469(1977)034<1149:tiopot>2.0.co;2, 1977.

Waliser, D. E., Li, J. L. F., Woods, C. P., Austin, R. T., Bacmeister, J., Chern, J., Del Genio, A., Jiang, J. H., Kuang, Z. M., Meng, H., Minnis, P., Platnick, S., Rossow, W. B., Stephens, G. L., Sun-Mack, S., Tao, W. K., Tompkins, A. M., Vane, D. G., Walker, C., and Wu, D.: Cloud ice: A climate model challenge with signs and expectations of progress, J Geophys Res-Atmos, 114, D00a21, DOI 10.1029/2008jd010015, 2009.

Wang, F., Guo, J. P., Zhang, J. H., Huang, J. F., Min, M., Chen, T. M., Liu, H., Deng, M. J., and Li, X. W.: Multi-sensor quantification of aerosol-induced variability in warm clouds over eastern China, Atmos Environ, 113, 1-9, 10.1016/j.atmosenv.2015.04.063, 2015.

Wang, J. D., Zhao, B., Wang, S. X., Yang, F. M., Xing, J., Morawska, L., Ding, A. J., Kulmala, M., Kerminen, V. M., Kujansuu, J., Wang, Z. F., Ding, D. A., Zhang, X. Y., Wang, H. B., Tian, M., Petaja, T., Jiang, J. K., and Hao, J. M.: Particulate matter pollution over China and the effects of control policies, Sci Total Environ, 584, 426-447, 10.1016/j.scitotenv.2017.01.027, 2017.

Winker, D. M., Hunt, W. H., and McGill, M. J.: Initial performance assessment of CALIOP, Geophys Res Lett, 34, L19803, DOI 10.1029/2007gl030135, 2007.

Wylie, D. P., Menzel, W. P., Woolf, H. M., and Strabala, K. I.: 4 Years of Global Cirrus Cloud Statistics Using Hirs, J Climate, 7, 1972-1986, Doi 10.1175/1520-0442(1994)007<1972:Fyogcc>2.0.Co;2, 1994.

Wylie, D. P., Jackson, D. L., Menzel, W. P., and Bates, J. J.: Trends in global cloud cover in two decades of HIRS observations, J Climate, 18, 3021-3031, Doi 10.1175/Jcli3461.1, 2005.

Zhao, B., Jiang, J. H., Gu, Y., Diner, D., Worden, J., Liou, K. N., Su, H., Xing, J., Garay, M., and Huang, L.: Decadal-scale trends in regional aerosol particle properties and their linkage to emission changes, Environ Res Lett, 12, 054021, 10.1088/1748-9326/aa6cb2, 2017a.

Zhao, B., Liou, K. N., Gu, Y., Li, Q. B., Jiang, J. H., Su, H., He, C. L., Tseng, H. L. R., Wang, S. X., Liu, R., Qi, L., Lee, W. L., and Hao, J. M.: Enhanced PM2.5 pollution in China due to aerosol-cloud interactions, Sci Rep-Uk, 7, 4453, 10.1038/s41598-017-04096-8, 2017b.

Figures

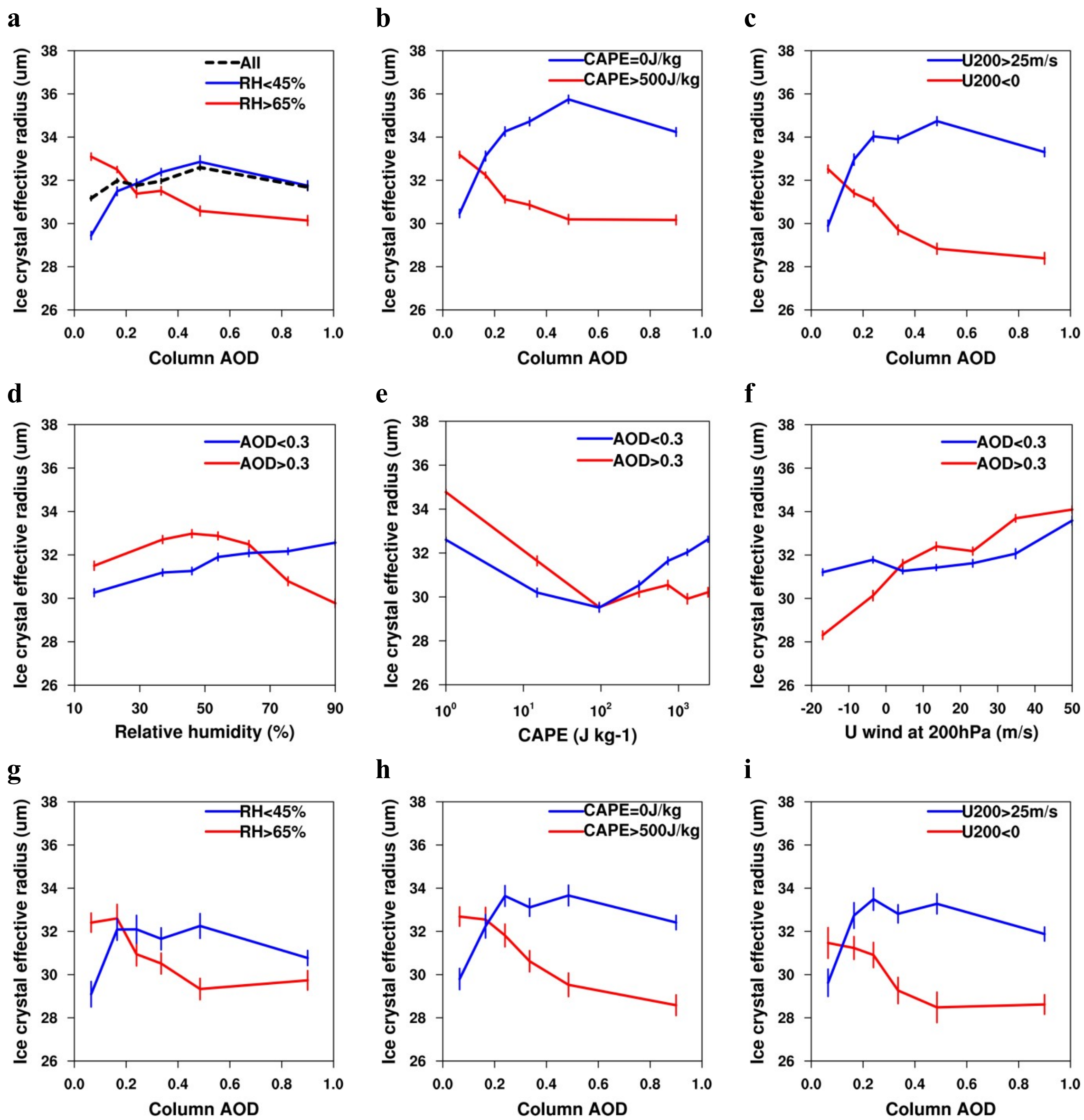

Figure 1. Influence of aerosols on ice crystal effective radius (R_{ei}) of ice clouds modulated by meteorological conditions. (a-c) Changes in R_{ei} with AOD for different ranges of (a) $RH_{100\text{-}440hPa}$, (b) CAPE, and (c) U200. (d-f) Changes in R_{ei} with (d) $RH_{100\text{-}440hPa}$, (e) CAPE, and (f) U200 for different ranges of AOD. (g-i) The same as (a-c) but for the profiles with dust aerosols only. The meteorological parameters and AOD are divided into 3 and 2 ranges containing similar numbers of data points, respectively; the curves for the medium meteorological range are not shown. The error bars denote the standard errors ($\sigma/\sqrt{N}$) of the bin average, where σ is the standard deviation and N is the sample number. The influences of other meteorological parameters are shown in Fig. S2. The total number of samples used in this figure is 5.68×10^4.

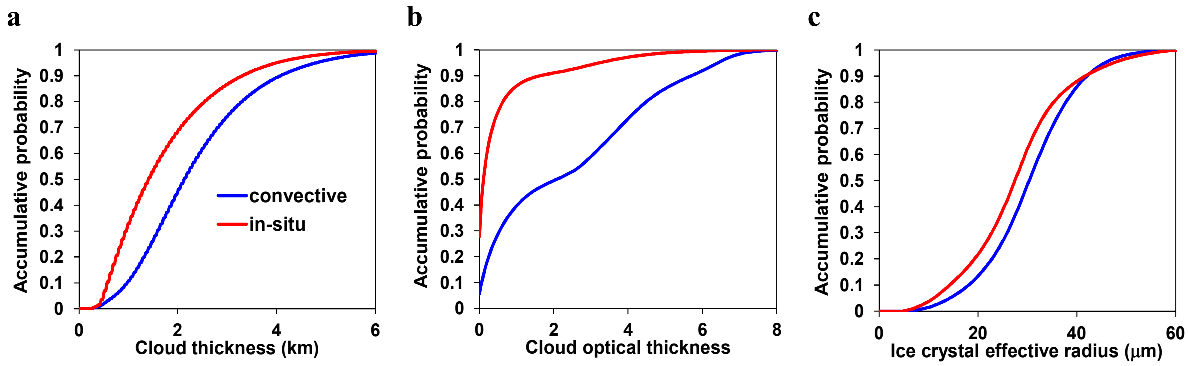

Figure 2. Accumulative probability distribution of the properties of two ice cloud types: (a) cloud thickness, (b) cloud optical thickness, and (c) R_{ei}.

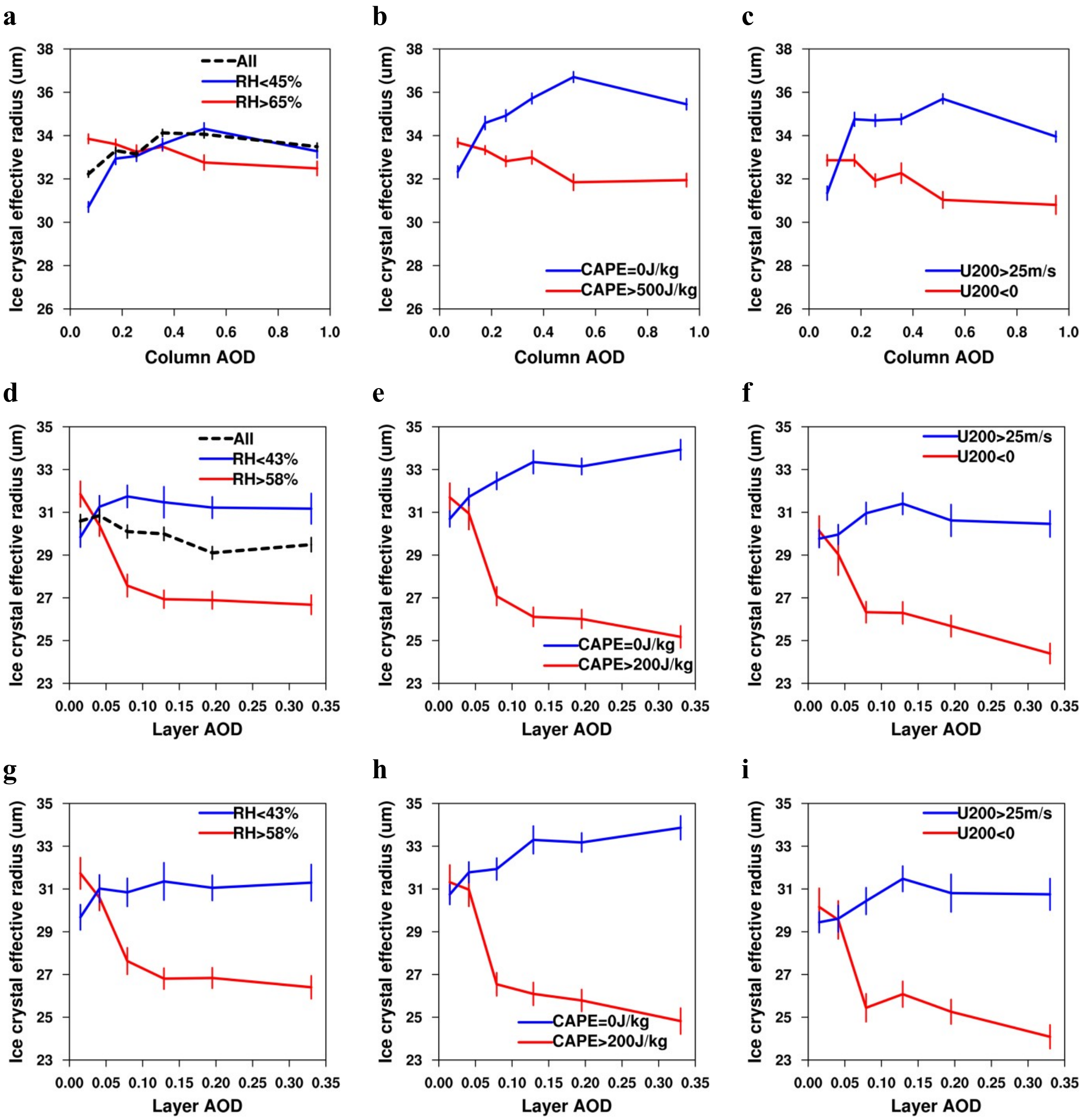

Figure 3. Changes in R_{ei} of convection-generated and in-situ ice clouds with aerosols. (a-c) Changes in R_{ei} of convection-generated ice clouds with AOD for different ranges of (a) $RH_{100\text{-}440hPa}$, (b) CAPE, and (c) U200. (d-f) Changes in R_{ei} of in-situ ice clouds with layer AOD for different ranges of (d) $RH_{100\text{-}440hPa}$, (e) CAPE, and (f) U200. (g-i) The same as (d-f) but for the profiles with dust aerosols only. The meteorological parameters are divided into 3 ranges containing similar numbers of data points, and the curves for the medium range are not shown. Note that we use column AOD and layer AOD mixed with ice clouds as proxies for aerosols interacting with convection-generated and in-situ ice clouds, respectively. The definition of error bars is the same as in Fig. 1. The total numbers of samples used for convection-generated and in-situ ice clouds are 2.73×10^4 and 1.09×10^4, respectively.

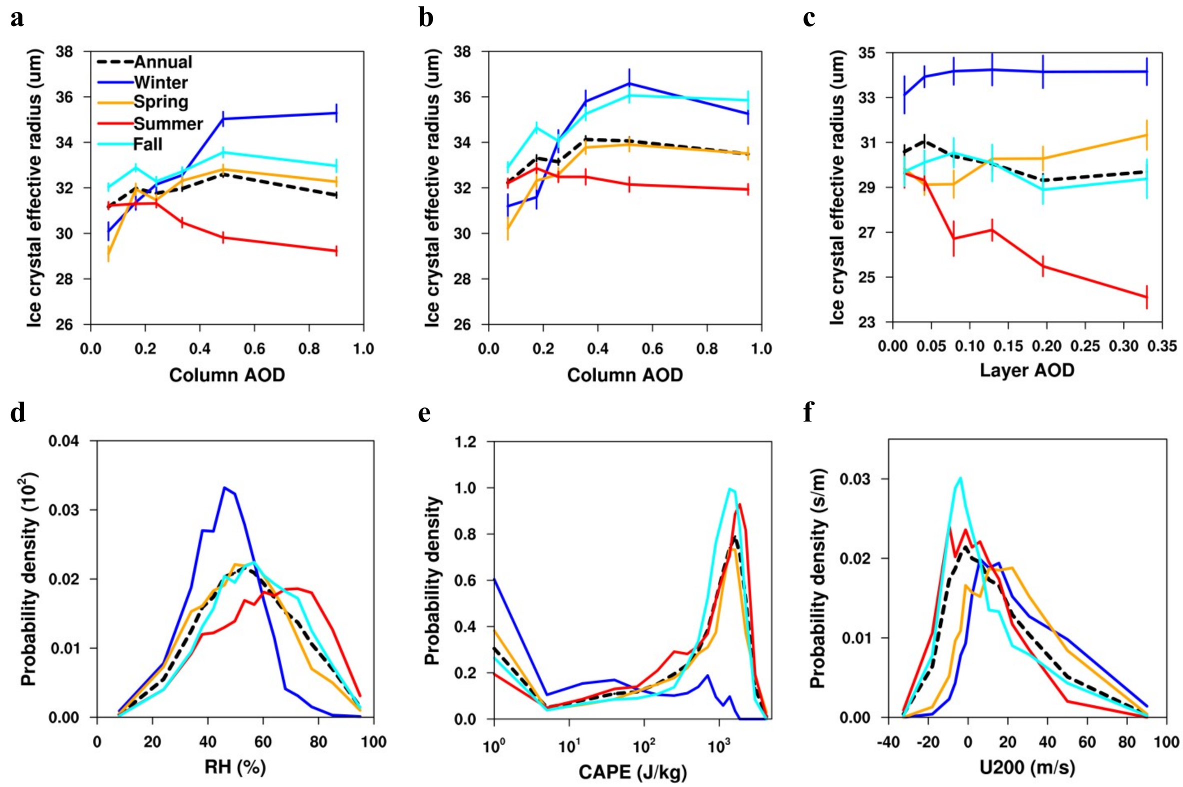

Figure 4. Changes in R_{ei} with AOD and the probability distribution of selected meteorological parameters as a function of season. (a-c) Changes in R_{ei} with AOD as a function of season for (a) all ice clouds, (b) convection-generated ice clouds, and (c) in-situ ice clouds. (d-f) The probability distribution of (d) $RH_{100\text{-}440hPa}$, (e) CAPE, and (f) U200 as a function of season. Definitions of season are as follows: Winter – December, January, and February; Spring – March, April, and May; Summer – June, July, and August; Fall – September, October, and November. The definition of error bars is the same as in Fig. 1. The total numbers of samples used in (a, d-f), (b), and (c) are 5.68×10^4, 2.73×10^4, and 1.09×10^4, respectively.

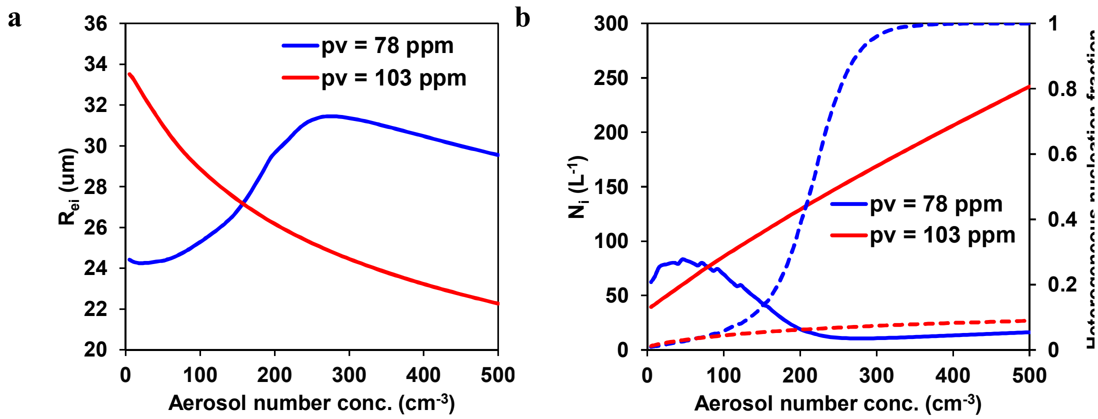

Figure 5. Simulated changes in (a) ice crystal effective radius (R_{ei}) and (b) ice crystal number concentration (N_i) and the fraction of ice crystal number produced by heterogeneous nucleation as a function of the total aerosol number concentration. Simulations are conducted for two initial water vapor mass mixing ratios (pv), an indicator of available water amount for ice formation. The ratios of externally mixed dust (deposition INP), coated dust (immersion INP), and sulfate (not INP) are prescribed with values of 0.75:0.25:10000 in all experiments.

Supplementary Information for

Impact of aerosols on ice crystal size

Bin Zhao[1], Kuo-Nan Liou[1], Yu Gu[1], Jonathan H. Jiang[2], Qinbin Li[1], Rong Fu[1], Lei Huang[1,2], Xiaohong Liu[3], Xiangjun Shi[3], Hui Su[2], and Cenlin He[1]

[1] Joint Institute for Regional Earth System Science and Engineering and Department of Atmospheric and Oceanic Sciences, University of California, Los Angeles, California 90095, USA.

[2] Jet propulsion Laboratory, California Institute of Technology, Pasadena, California 91109, USA.

[3] Department of Atmospheric Science, University of Wyoming, Laramie, Wyoming 82071, USA.

Correspondence to: Bin Zhao (zhaob1206@ucla.edu) and Yu Gu (gu@atmos.ucla.edu)

Figures and Tables

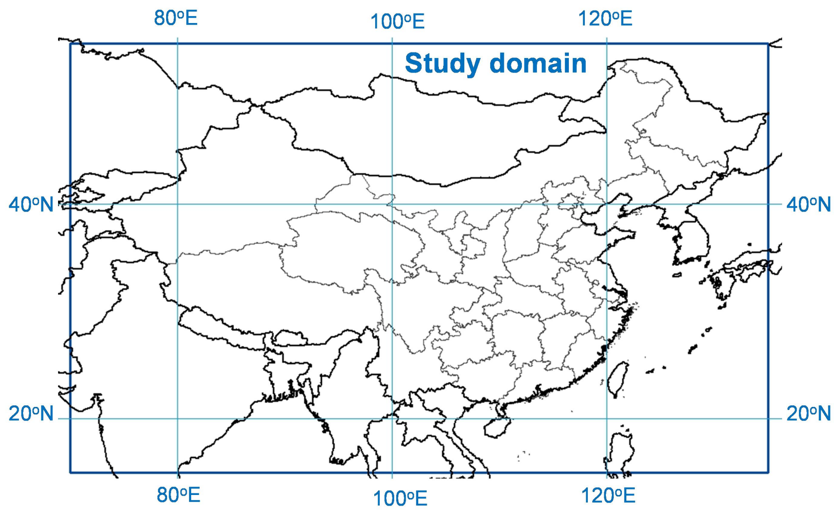

Figure S1. The spatial domain of this study: 15º-55º N, 70º-135º E.

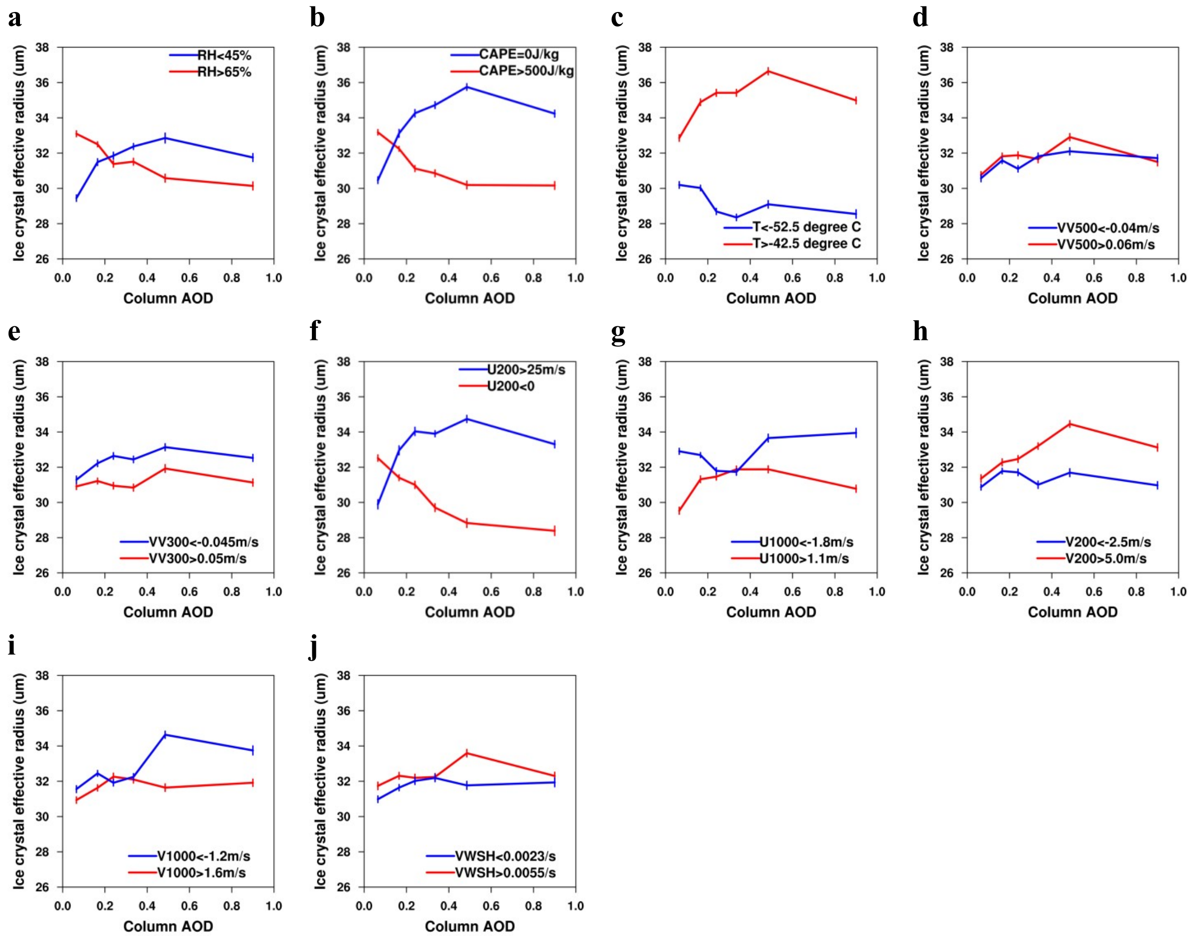

Figure S2. Changes in R_{ei} as a function of AOD for different ranges of (a) relative humidity averaged between 100 hPa and 440 hPa ($RH_{100\text{-}440hPa}$), (b) the convective available potential energy (CAPE), (c) the middle cloud layer temperature (T_{mid}), (d) the vertical velocity at 500 hPa (VV500), (e) the vertical velocity at 300 hPa (VV300), (f) the U-components of wind speed at 200 hPa (U200), (g) the U-components of wind speed at 1000 hPa (U1000), (h) the V-components of wind speed at 200 hPa (V200), (i) the V-components of wind speed at 1000 hPa (V1000), (j) and the vertical wind shear (VWSH) at potential vorticity surface of 2×10^{-6} deg K m^2 kg^{-1} s^{-1}. The meteorological parameters are divided into 3 ranges containing similar numbers of data points, and the curves for the medium meteorological range are not shown. The definition of error bars is the same as in Fig. 1 in the main text. The total number of samples used in this figure is 5.68×10^4.

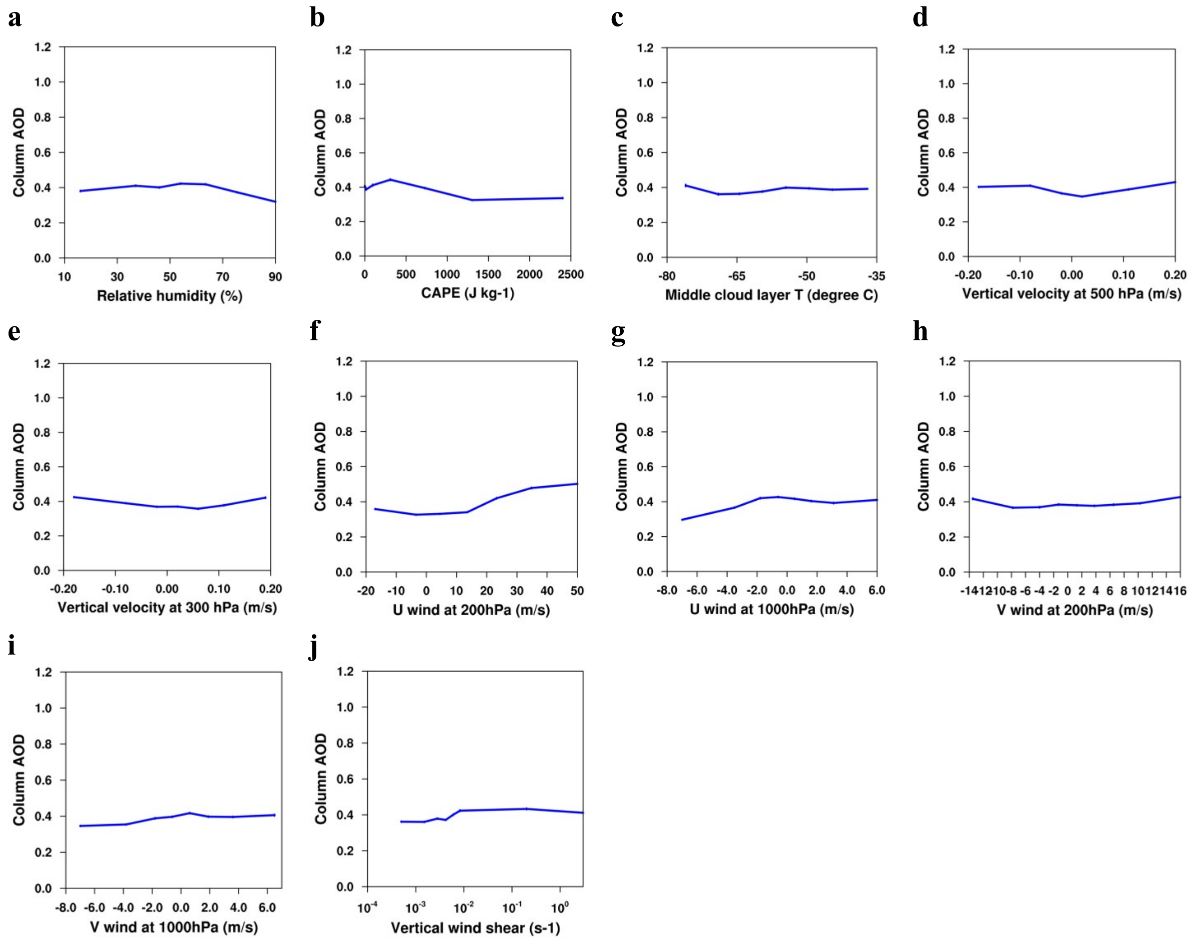

Figure S3. Changes in AOD as a function of meteorological parameters: (a) $RH_{100\text{-}440hPa}$, (b) CAPE, (c) T_{mid}, (d) VV500, (e) VV300, (f) U200, (g) U1000, (h) V200, (i) V1000, and (j) VWSH at the potential vorticity surface of 2×10^{-6} deg K m^2 kg^{-1} s^{-1}. The definition of error bars is the same as in Fig. 1 in the main text. Note that the error bars in some panels are very small and hence not visible. The total number of samples used in this figure is 5.68×10^4.

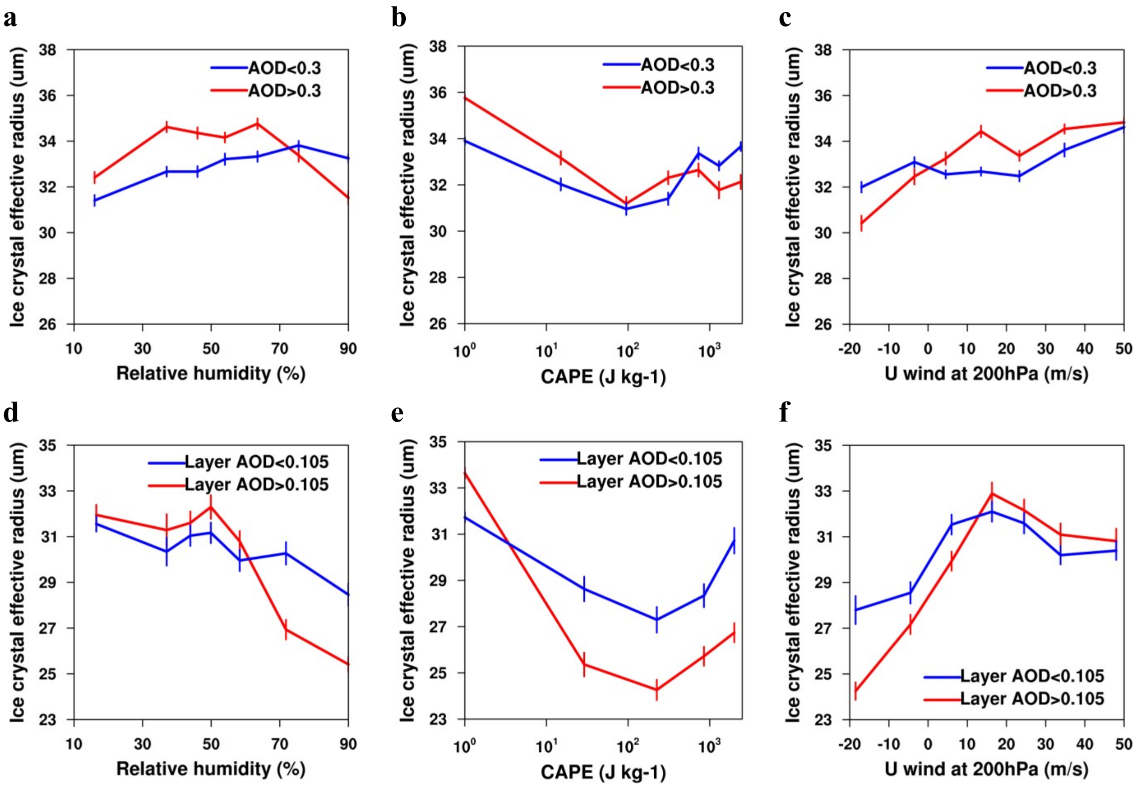

Figure S4. Changes in R_{ei} with meteorological parameters for different ranges of aerosol loading. (a-c) Changes in R_{ei} of convection-generated ice clouds with (a) $RH_{100\text{-}440hPa}$, (b) CAPE, and (c) U200 for different ranges of AOD. (d-f) Changes in R_{ei} of in-situ ice clouds with (d) $RH_{100\text{-}440hPa}$, (e) CAPE, and (f) U200 for different ranges of layer AOD. All samples are divided into two AOD ranges containing similar sample numbers. The definition of error bars is the same as in Fig. 1. The total numbers of samples used for convection-generated and in-situ ice clouds are 2.73×10^4 and 1.09×10^4, respectively.

Table S1. Datasets used in this study.

Satellite/ Sensor	Product	Variable	Horizontal resolution
Aqua/MODIS	MYD04 (Level 2, Collection 6)	Column AOD	10 km × 10 km
	MYD06 (Level 2, Collection 6)	Cloud effective radius, cloud phase (determined by the "cloud optical property" algorithm), primary cloud retrieval outcome	1 km × 1 km
CALIPSO/ CALIOP	05kmMLay (Level 2, Version 4.10)	Aerosol/cloud layer number, layer base temperature, middle layer temperature, layer top/base height, layer aerosol/cloud optical depth, feature classification flags, CAD score, extinction QC	5 km along-track
	05kmAPro (Level 2, Version 4.10)	Vertically resolved pressure, relative humidity, and temperature	5 km along-track
--	NCEP ds083.2	Vertically resolved vertical velocity and wind speed; CAPE, wind shear	1º × 1º

Table S2. Correlation coefficients between various meteorological parameters.

	$RH_{100\text{-}440hPa}$	CAPE	U200	T_{mid}
$RH_{100\text{-}440hPa}$	--	0.514	-0.535	-0.352
CAPE	0.514	--	-0.623	-0.390
U200	-0.535	-0.623	--	0.502
T_{mid}	-0.352	-0.390	0.502	--

Note: $p < 0.01$ for all cases. $RH_{100\text{-}440hPa}$, relative humidity averaged between 100 hPa and 440 hPa; CAPE, convective available potential energy; U200, U-components of wind speed at 200 hPa; T_{mid}, middle cloud layer temperature.